JOURNAL OF GEOPHYSICAL RESEARCH, VOL. 105, NO. D18, PAGES 22,869–22,896, SEPTEMBER 27, 2000

Linking local air pollution to global chemistry and climate

Monika Mayer, Chien Wang, Mort Webster, and Ronald G. Prinn

Joint Program on the Science and Policy of Global Change, Massachusetts Institute of Technology, Cambridge

Abstract. We have incorporated a reduced-form urban air chemistry model in the Massachusetts Institute of Technology's two-dimensional land and ocean resolving coupled chemistry-climate model. The computationally efficient reduced-form urban model was derived from the California Institute of Technology–Carnegie Institute of Technology (at Carnegie Mellon University) Urban Airshed Model by employing the probabilistic collocation method. To study the impact of urban air pollution on global chemistry and climate, we carried out three simulations, each including or excluding the reduced-form urban model for the time period from 1977 to 2100. All three runs use identical total emissions; however, in the two runs involving the reduced-form urban model, the emissions assigned to urban areas are allocated in different ways, depending on the scenario assumed for the future development of polluted urban areas. These two simulations are compared to the reference, which does not utilize the reduced-form urban model. We find that the incorporation of urban air chemistry processes leads to lower global tropospheric NO_x, ozone, and OH concentrations, but a higher methane mole fraction, than in the reference. The tropospheric mole fraction of CO is altered either up or down depending on the projections of urban emissions. The global mean surface temperature is affected very little by implementation of the reduced-form urban model because predicted increases in CH_4 are offset in part by decreases in O_3, leading to only small changes in overall radiative forcing.

1. Introduction

Urban air pollution is not only a regional issue; it is also a global atmospheric chemistry issue. Urban air pollution can alter concentrations of greenhouse gases such as tropospheric ozone directly [e.g., *Wang et al.*, 1986; *Hauglustaine and Granier*, 1995] or indirectly via changes in the OH free radical concentration [*Levy*, 1972] and NO_x concentration [*Lin et al.*, 1988; *Chameides et al.*, 1992; *Brasseur et al.*, 1996; *Pickering et al.*, 1996]. In order to study the impact of urban air pollution on global atmospheric chemistry and climate, a global model interactively coupling submodels of climate, atmospheric chemistry, and economic development can in principle be used. However, atmospheric chemical processes over urban areas are highly nonlinear and differ from those over nonurban areas in many respects. In addition, lifetimes of many trace species involved, especially NO_x and nonmethane volatile organic compounds (NMVOC), are very short ($\leq$ 1 day), and sources of emissions vary on short space scales, so that a spatial resolution $\leq$ 5 km is required for simulations of urban chemical processes in global models. The spatial resolution of most global-scale atmospheric chemistry models currently available is typically > 200 km (in which case urban chemistry is indeed a subgrid-scale process), and the models' chemical simulations resemble nonurban chemical processes more closely than urban chemical processes because of the averaging nature of chemical properties over the model grid volume. In order to appropriately model O_3 and OH on a global scale, a global three-dimensional (3-D) model should have the following characteristics: (1) a resolution < 100 km (1 degree) because of the short lifetime of NO_x (a few days); (2) prognostic rather than diagnostic O_3-HO_x-NO_x-CO-CH_4 background chemistry (especially for CH_4, the simulation should be transient and longer than the lifetime of CH_4); (3) inclusion of NMVOC chemistry; and (4) reasonable high-resolution multiyear global emission inventories for all necessary anthropogenic and biogenic sources. Unfortunately, computational constraints and the lack of global high-resolution emission inventories currently limit our ability to model O_3 and OH over time periods on the order of decades. The impact of urban air pollution on global atmospheric chemistry and climate can be determined in several ways, each having its own weaknesses and strengths.

This paper presents a new approach for including urban chemical subgrid-scale processes in a global interactive chemistry-climate model (specifically, that of *Wang et al.* [1998] and *Prinn et al.* [1999]) by adding a computationally efficient, "reduced-form" model for urban air chemistry including NMVOC. This model consists of a set of analytical expressions derived from the parent urban airshed model, which approximate the predictions of the parent model. This significant improvement over the previous model allows us to study the impact of local air pollution on global climate and air chemistry, especially on changes in the global concentrations of tropospheric O_3, NO_x, CO, CH_4, and OH, and to improve the model's predictions regarding tropospheric chemical composition.

This paper first describes the derivation of the reduced-form model for urban air chemistry and its implementation. The impact on global chemistry and climate of extending the chemistry model with the reduced-form model is then

Paper number 2000JD900307.
0148-0227/00/2000JD900307$09.00

Table 1. Gaseous Phase Chemical Reactions Included in the Global Chemistry-Climate Model[a]

Number	Reaction	A, k_0, or k_∞	E/R or $f(T)$	References
(R1)	$O_3 + h\nu \rightarrow O(^1D) + O_2$			1
(R2)	$O(^1D) + H_2O \rightarrow 2OH$	2.2×10^{-10}		1
(R3)	$O(^1D) + N_2 \rightarrow O + N_2$	1.8×10^{-11}	107	1
(R4)	$O(^1D) + O_2 \rightarrow O + O_2$	3.2×10^{-11}	67	1
(R5)	$CO + OH \rightarrow H + CO_2$	$1.5 \times 10^{-13}[1 + 0.6\,p(\text{atm})]$		1
(R6)	$H + O_2 + M \rightarrow HO_2 + M$	$k_0 = 6.2 \times 10^{-32}$	$(T/300)^{-1.6}$	2
		$k_\infty = 7.5 \times 10^{-11}$		2
(R7)	$HO_2 + NO \rightarrow OH + NO_2$	3.7×10^{-12}	240	1
(R8)	$NO_2 + h\nu \rightarrow NO + O$			1
(R9)	$O + O_2 + M \rightarrow O_3 + M$	$k_0 = 5.6 \times 10^{-34}$	$(T/300)^{-2.8}$	1
(R10)	$HO_2 + O_3 \rightarrow OH + 2O_2$	1.1×10^{-14}	-500	2
(R11)	$OH + O_3 \rightarrow HO_2 + O_2$	1.6×10^{-12}	-940	2
(R12)	$NO + O_3 \rightarrow NO_2 + O_2$	2.0×10^{-12}	-1400	2
(R13)	$NO_2 + OH + M \rightarrow HNO_3 + M$	$k_0 = 2.6 \times 10^{-30}[N_2]$	$(T/300)^{-3.2}$	2
		$k_\infty = 2.4 \times 10^{-11}$	$(T/300)^{-1.3}$	2
(R14)	$NO_2 + O_3 \rightarrow NO_3 + O_2$	1.2×10^{-13}	-2450	1
(R15)	$NO_3 + NO_2 + M \rightarrow N_2O_5 + M$	$k_0 = 2.2 \times 10^{-30}[N_2]$	$(T/300)^{-3.9}$	2
		$k_\infty = 1.5 \times 10^{-12}$	$(T/300)^{-0.7}$	2
(R16)	$HO_2 + HO_2 \rightarrow H_2O_2 + O_2$	2.3×10^{-13}	600	2, 3
(R17)	$H_2O_2 + h\nu \rightarrow 2OH$			1
(R18)	$H_2O_2 + OH \rightarrow HO_2 + H_2O$	2.9×10^{-12}	-160	1
(R19)	$HO + HO_2 \rightarrow H_2O + O_2$	4.8×10^{-11}	250	2
(R20)	$HO + HO \rightarrow H_2O + O$	4.2×10^{-12}	-240	2
(R21)	$HO + HO + M \rightarrow H_2O_2 + M$	$k_0 = 6.9 \times 10^{-31}$	$(T/300)^{-0.8}$	2
		$k_\infty = 1.5 \times 10^{-11}$		2
(R22)	$CH_4 + OH \rightarrow CH_3 + H_2O$	2.65×10^{-12}	-1800	2
(R23)	$CH_3 + O_2 + M \rightarrow CH_3O_2 + M$	$k_0 = 4.5 \times 10^{-31}$	$(T/300)^{-3}$	2
		$k_\infty = 1.8 \times 10^{-12}$	$(T/300)^{-1.7}$	2
(R24)	$CH_3O_2 + NO \rightarrow CH_3O + NO_2$	4.2×10^{-12}	180	1
(R25)	$CH_3O + O_2 \rightarrow CH_2O + HO_2$	3.9×10^{-14}	-900	2
(R26)	$CH_3O_2 + HO_2 \rightarrow CH_3O_2H + O_2$	3.8×10^{-13}	780	1
(R27)	$CH_3O_2H + h\nu \rightarrow CH_3O + OH$			1
(R28)	$CH_3O_2H + OH \rightarrow CH_3O_2 + H_2O$	1.9×10^{-12}	190	1
(R29)	$CH_2O + h\nu \rightarrow CHO + H$			1
(R30)	$CH_2O + OH \rightarrow CHO + H_2O$	1.0×10^{-11}		2
(R31)	$CHO + O_2 \rightarrow CO + HO_2$	3.5×10^{-12}	140	2
(R32)	$SO_2 + OH + M \rightarrow HOSO_2 + M$	$k_0 = 3.0 \times 10^{-31}$	$(T/300)^{-3.3}$	2
		$k_\infty = 1.5 \times 10^{-12}$		2
(R33)	$HOSO_2 + O_2 \rightarrow HO_2 + SO_3$	1.3×10^{-12}	-330	1
(R34)	$SO_3 + H_2O \rightarrow H_2SO_4$	2.4×10^{-15}		2
(R35)	$CFCl_3 + O(^1D) \rightarrow$ products			1, 4[b]
(R36)	$CFCl_3 + h\nu \rightarrow$ products			1, 4[b]
(R37)	$CF_2Cl_2 + O(^1D) \rightarrow$ products			1, 4[b]
(R38)	$CF_2Cl_2 + h\nu \rightarrow$ products			1, 4[b]
(R39)	$N_2O + h\nu \rightarrow N_2 + O(^1D)$			1, 4[b]
(R40)	$N_2O + O(^1D) \rightarrow 2NO$			1, 4[b]
(R41)	$N_2O + O(^1D) \rightarrow N_2 + O_2$			1, 4[b]
(R42)	$CF_3CH_2F + OH \rightarrow CF_3CHF + H_2O$	1.7×10^{-12}	1750	2

[a] from *Wang et al.* [1998]; References are 1, *Atkinson et al.* [1992]; 2, *DeMore et al.* [1994]; 3, *Stockwell* [1995]; 4, *Wang et al.* [1998]. For bimolecular reactions, rate constants (cm^3/molecule/s) can be derived by $k(T) = A \exp\{(-E/R)(1/T)\}$. For termolecular reactions, rate constants (cm^3/molecule/s) can be derived by $k(T) = [k_0(T)[M]/(1 + k_0(T)[M]/k_\infty(T))]\ 0.6^a$. Here $a = 1/\{1 + [\log 10(k_0(T)[M]/k_\infty(T))]^2\}$, $k_0(T) = k_0 f(T)$, and $k_\infty(T) = k_\infty f(T)$.

[b] Parameterized, current version of the model does not include predictions of stratospheric ozone chemistry.

Table 2. Aqueous Phase Chemical Reactions Included in the Global Chemistry-Climate Model[a]

Number	Reaction	K_{298}, M or M atm^{-1}	$-\Delta H/R$, K	References
(R43)	H_2SO_4 (g) ⇔ H_2SO_4 (aq)	infinite		
(R44)	H_2SO_4(aq) ⇔ HSO_4^- + H^+	1.00×10^3		1
(R45)	HNO_3 (g) ⇔ HNO_3 (aq)	$2.10 \times 10^5 F_1$	8700	2
(R46)	HNO_3(aq) ⇔ NO_3^- + H^+	1.54×10^1	8700	2
(R47)	CH_2O(g) ⇔ $CH_2(OH)_2$	3.10×10^3	6500	3
(R48)	SO_2 (g) ⇔ SO_2 (aq)	$1.20 F_2$	3100	4
(R49)	SO_2(aq) ⇔ HSO_3^- + H^+	1.23×10^{-2}	1960	4
(R50)	HSO_3^- ⇔ SO_3^{2-} + H^+	6.61×10^{-8}	1500	4
(R51)	H_2O_2(g) ⇔ H_2O_2 (aq)	$7.40 \times 10^4 F_3$	6615	5
(R52)	H_2O_2(aq) ⇔ HO_2^- + H^+	2.20×10^{-12}	-3730	4
(R53)	OH(g) ⇔ OH(aq)	2.50×10^1	5280	6
(R54)	HO_2(g) ⇔ HO_2(aq)	$2.30 \times 10^3 F_4$	6640	2
(R55)	HO_2(aq) ⇔ O_2^- + H^+	3.50×10^{-5}		1

[a] from *Wang et al.* [1998]; References are 1, *Perrin* [1982]; 2, *Schwartz* [1984]; 3, *Pandis and Seinfeld* [1989]; 4, *Smith and Martell* [1976]; 5, *Lind and Kok* [1986]; 6, *Jacob* [1986]. The equilibrium constants are defined by $K = K_{298} \exp\{(-\Delta H/R)(1/T-1/298)\}$. Functions are defined as $F_1 = (1 + R46/[H^+])$, $F_2 = (1 + R49/[H^+] + R49 \cdot R50/[H^+]^2)$, $F_3 = (1 + R52/[H^+])$, and $F_4 = (1 + R55/[H^+])$.

discussed, followed by some conclusions regarding the success of this approach.

2. Model Overview

The Massachusetts Institute of Technology (MIT)'s Integrated Global System Model [*Prinn et al.*, 1999] includes an economic development model (the Emission Predictions and Policy Analysis (EPPA) Model) [*Yang et al.*, 1996], a two-dimensional land and ocean resolving (2D-LO) interactive chemistry-climate model [*Wang et al.*, 1998; *Sokolov and Stone*, 1998], a terrestrial ecosystems model [*Xiao et al.*, 1997], and a natural emissions model. The EPPA model divides the world into 12 regions: the United States, Japan, European Community, other countries of the Organization for Economic Cooperative Development, central and eastern Europe, the former Soviet Union, energy-exporting countries, China, India, dynamic Asian economies, Brazil, and the rest of the world. The EPPA model is a recursive-dynamic computable general equilibrium (CGE) model that calculates in 5-year time steps the anthropogenic emissions of CO_2, CH_4, N_2O, CFCs, NO_x, CO, and SO_x as well as a variety of economic variables. When driven with these anthropogenic emissions as well as calculated or estimated natural emissions, the 2D-LO atmospheric chemistry-climate model predicts various climate variables as well as zonally averaged mole fractions of major chemically and radiatively important trace species in the atmosphere as a function of time, latitude, and altitude [*Wang et al.*, 1998]. The chemistry and climate submodels are fully interactive. Specifically, the transport of 18 chemical species ($CFCl_3$, CF_2Cl_2, N_2O, O_3, CO, CO_2, NO, NO_2, N_2O_5, HNO_3, CH_4, HCHO, SO_2, H_2SO_4, hydrofluorocarbons (HFCs), perfluorocarbons (PFCs), sulfur hexafluoride (SF_6), and water vapor) is driven by dynamical variables predicted by the climate submodel. The calculations of 55 gaseous and aqueous phase reactions are based on temperatures, radiative fluxes, and precipitation rates computed by the climate model.

The gas-phase chemistry of the coupled chemistry-climate model consists of three parts: tropospheric O_3-HO_x-NO_x-CO-CH_4 reactions (following *Crutzen and Zimmermann* [1991]); tropospheric SO_2 sulfate reactions; and stratospheric chlorofluorocarbon and N_2O removal reactions [*Wang et al.*, 1998]. The current version of the global coupled chemistry-climate model does not include anthropogenic or biogenic NMVOC chemistry. Tables 1 and 2 list all 55 gaseous and aqueous phase reactions included in the global model, which uses annually averaged emissions. For 1990, the annual global (anthropogenic plus natural) emissions are 7 Pg C as CO_2, 0.6 Pg CH_4, 13 Tg N as N_2O, no HFCs, 19.9 Gg PFCs, 9.6 Gg SF_6, 0.25 Tg $CFCl_3$, 0.4 Tg CF_2Cl_2, 0.72 Pg C as CO, 48 Tg N as NO_x, and 84 Tg S as SO_2, respectively. In 2100 we use the following global emission rates: 21 Pg C as CO_2, 1.1 Pg CH_4, 19 Tg N as N_2O, 1.7 Tg HFCs, 20.5 Gg PFCs, 9.6 Gg SF_6, 21 Pg C as CO, 92 Tg N as NO_x, and 125 Tg S as SO_2, respectively. $CFCl_3$ and CF_2C_{l2} emissions are zero after 2000. Detailed emissions data are provided by *Wang et al.* [1998], except for HFCs, PFCs, and SF_6, which are documented by *Reilly et al.* [1999].

Compared to data obtained by ozone sounding, the global coupled chemistry-climate model reproduces the general climatology of the latitudinal distribution of ozone outside polluted regions, but underestimates ozone mole fractions in northern midlatitudes [*Wang et al.*, 1998]. The OH distributions predicted by the global model provide reasonable simulations of OH-sensitive species like CH_4 and CO, compared with Atmospheric Lifetime Experiment/Global Atmospheric Gases Experiment/Advanced Global Atmospheric Gases Experiment network measurements. The globally averaged OH concentration in the troposphere predicted by the model (10.4×10^5 radicals/cm^3) is close to the estimate made by Prinn et al. [1995] based on CH_3CCl_3 measurements ($(9.7 \pm 0.6) \times 10^5$ radicals/cm^3). For more details, see *Wang et al.* [1998].

Predicted mole fractions of CO_2, CH_4, N_2O, two CFCs ($CFCl_3$ and CF_2Cl_2), tropospheric O_3, HFCs, PFCs, SF_6, and

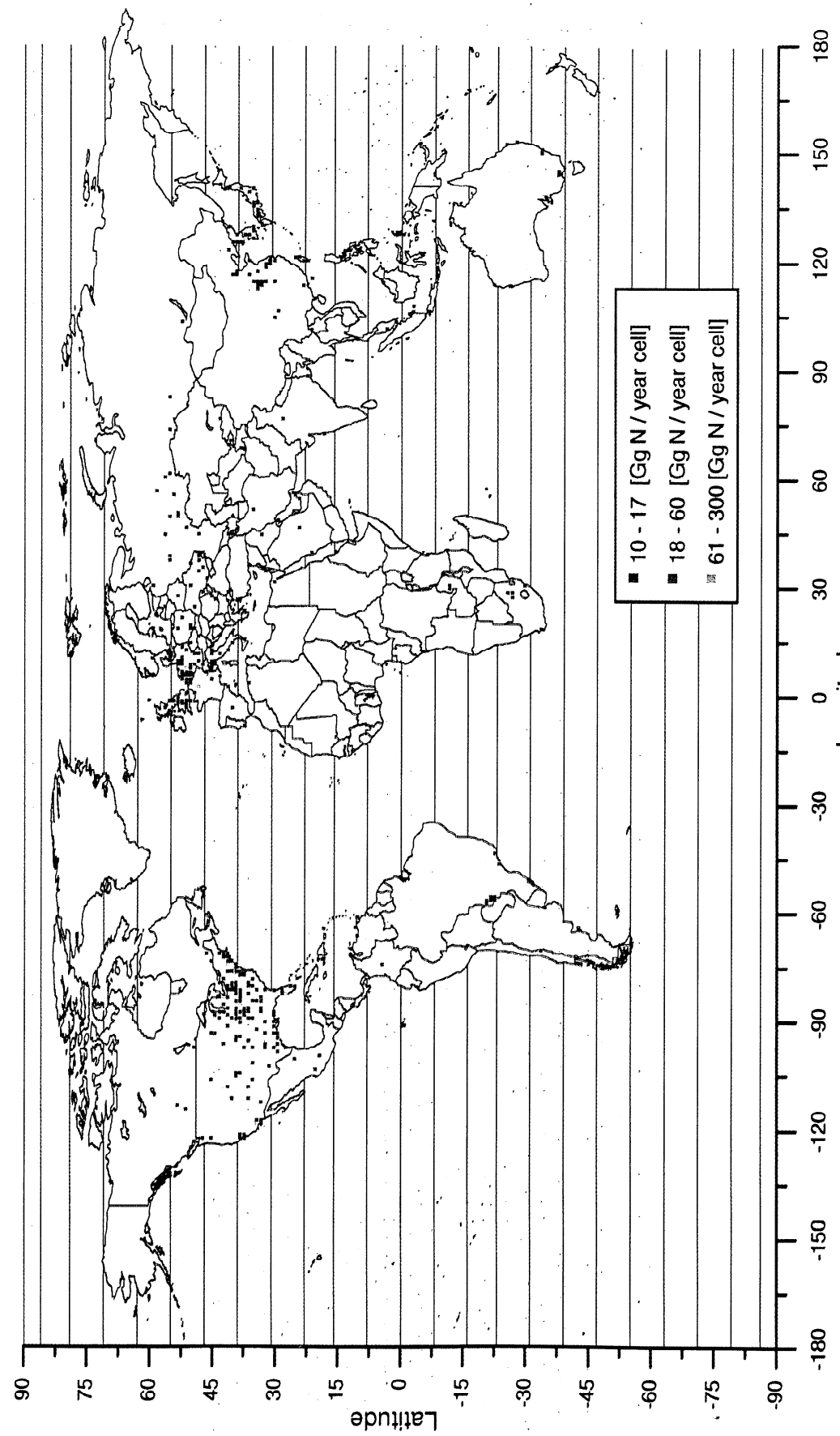

Plate 1. Global distribution of polluted urban areas represented by NO_x emissions of the EDGAR version 2.0 inventory for 1990. The horizontal lines demarcate the 24 latitudinal bands of the 2D-LO coupled chemistry-climate model.

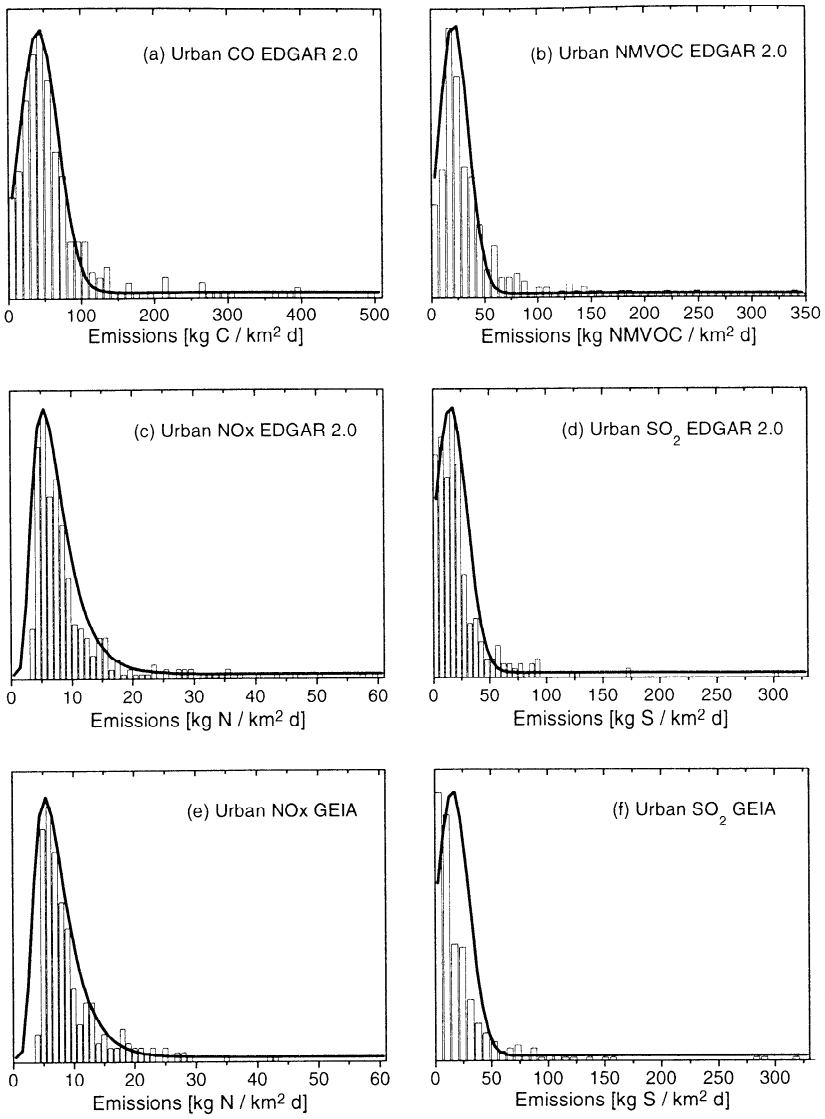

Figure 1. PDF data and fits for emissions in polluted urban areas of (a) CO, (b) NMVOC, (c) NO_x, and (d) SO_2 derived from the EDGAR inventory, and (e) NO_x and (f) SO_2 derived from the GEIA inventory. The CO, NMVOC, and SO_2 PDF data are fitted with normal distributions, and the NO_x PDF data are fitted with a lognormal distribution. The analytical curves used to fit the GEIA inventory data are the same as these used for the EDGAR data.

sulfate aerosols are used to calculate radiative forcing in the climate submodel. Outputs from the chemistry-climate model such as CO_2 concentration, precipitation, surface temperature, and cloud coverage are then utilized by the ecosystem model to calculate important biogeochemical fluxes, including net primary and ecosystem production [*Xiao et al.*, 1998].

3. Reduced-Form Model for Urban Atmospheric Chemistry

The 2D-LO global atmospheric chemistry and climate model in its original version [*Wang et al.*, 1998] cannot be used to explicitly investigate the interaction between local air pollution and global atmospheric chemistry because (1) the resolution of the model is much too coarse to resolve urban areas, and (2) the model does not include NMVOC chemistry, which is essential for modeling photochemical smog.

The research reported here attempts to solve this problem by creating and implementing in the 2D-LO model a computationally efficient, reduced form of an urban airshed model that is adequate for air quality simulations. Our version of the reduced-form model is significantly improved over the earlier model of *Calbo et al.* [1998]. Specifically, the new version includes better input data as well as improved numerical approaches.

3.1. Definition and Characterization of Polluted Urban Areas

In order to derive a numerically efficient, yet reasonably realistic, parameterization to insert in global models, we assume that all urban areas in our simulation have the same basic set of chemical reactions and the same size (200 km x 200 km x 2 km). However, meteorological conditions and

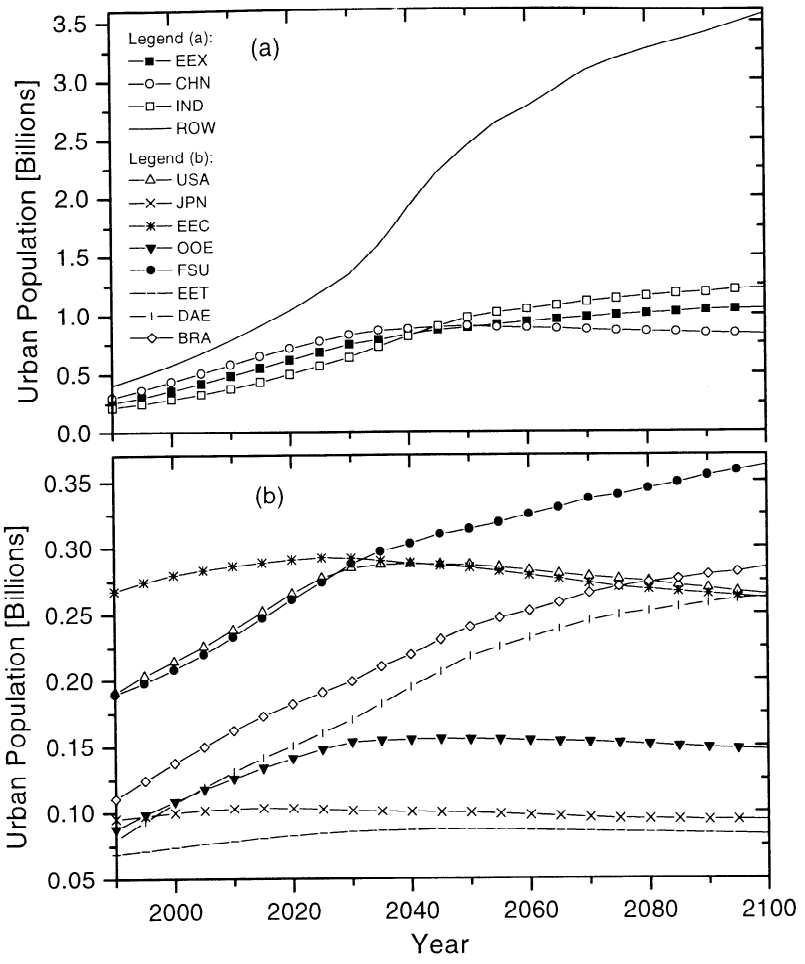

Figure 2. Urban population projections from 1990 through 2100 for several regions of the economic (EPPA) model; for acronyms of the EPPA regions see note to Table 4.

emissions (provided in our case by the climate submodel and the EPPA submodel, respectively) differ significantly for urban areas in each latitudinal band, and such important factors as these are taken into account by our model, to the extent possible.

In the present study, polluted areas are characterized by high concentrations of NO_x and NMVOC. Assuming that high mole fractions of these pollutants correlate with high emissions of NO_x and NMVOC, we first employed a global emissions inventory to identify urban areas. Specifically, we used the Emission Database for Global Atmospheric Research (EDGAR) version 2.0 of 1990 [*Olivier et al.*, 1995]. This data set contains, along with other inventories, emissions data for anthropogenic NO_x, CO, NMVOC, and SO_x for grid cells having a spatial resolution of 1° x 1°.

A grid cell is counted as an urban area if the EDGAR daily NO_x emissions within it exceed 5 kg N/(d km^2) and the ratio of NMVOC to NO_x emissions ranges from 1 to 9 [*Sillman et al.*, 1990]. Plate 1 shows the derived global distribution of highly polluted urban areas in 1990 and the 24 latitudinal bands of the 2D-LO model. Not only the geographic distribution of NO_x emissions, but the range of emission rates in each grid cell and the probability density function (PDF) of the emission rates can be obtained. All emission rates attributed to urban NO_x-emitting grid cells were plotted in the form of a histogram to determine the PDF of urban NO_x emissions. The histogram was then fitted with an analytical function. To derive the PDFs of urban emissions of NMVOC, CO, and SO_2, the map of urban areas derived from the NO_x inventory was applied to the individual EDGAR inventories. Histograms of the emission rates assigned to urban NMVOC, CO, and SO_2 grid cells were created and also fitted with analytical functions. Figure 1 shows the PDFs of NO_x, CO, SO_2, and NMVOC, together with their analytical fits. The CO, NMVOC, and SO_2 data are fitted with normal distributions, and the NO_x data with a lognormal distribution. We will use these fits to define the ranges of possible emission rates per unit area when deriving the reduced-form urban model. We also used the Global Emissions Inventory Activity (GEIA) data set for 1985 [*Bouscaren*, 1990; *Carnovale et al.*, 1992; *Dignon*, 1992; *Kato and Akimoto*, 1992; *Saeger et al.*, 1989; *Sandnes and Styve*, 1992; *Spiro et al.*, 1992; *Wagner et al.*, 1986] to derive emission PDFs. The GEIA data set has the same resolution as the EDGAR data set but includes no inventories for anthropogenic CO and NMVOC emissions. To derive the emission PDFs using the GEIA data set, only the criterion of high NO_x emissions was applied. We believe this approach to be reasonable based on results derived from the EDGAR data set: more than 98% of the high-NO_x emissions grid cells have high NMVOC emissions. The most likely

Table 3. The Percentage of Global Emissions Attributable to Urban Areas for NO_x, SO_2, CO, and NMVOCs, and the Number of Polluted Urban Areas in Several Latitude Bands, Derived From the EDGAR 1990 Emissions Inventory for the Northern and Southern Hemispheres

Latitude	NO_x, %	SO_2, %	CO, %	NMVOC, %	Urban Areas
55°-63°N	38	36	32	21	18
47°-55°N	51	43	37	45	69
39°-47°N	52	41	40	44	93
31°-39°N	49	46	34	40	99
23°-31°N	30	24	13	13	34
16°-23°N	21	26	9	13	9
8°-16°N	5	8	3	4	3
0°-8°N	6	4	2	4	3
0°-8°S	2	3	2	3	1
8°-16°S	14	3	13	10	2
16°-23°S	14	6	13	13	7
23°-31°S	32	33	14	24	6
31°-39°S	47	54	31	43	8

exception would be a grid cell dominated by power plants that emit substantial NO_x but negligible NMVOC. Figure 1 plots the PDFs and the analytical fits of the GEIA data. For NO_x and SO_2 urban emissions the EDGAR and GEIA data have a similar distribution, and as an approximation we could use the analytical PDFs derived from the EDGAR data to fit the GEIA data.

The quantities of total global emissions attributable to urban areas (hereinafter "urban emissions") for each species at different latitudinal bands can also be calculated. Table 3 lists the percentage of global emissions from urban areas (the "partition" between urban and nonurban emissions) along with the number of urban areas in each latitudinal band of the 2D-LO coupled atmospheric chemistry-climate model for 1990. The percentages of urban emissions in each latitudinal band derived from the EDGAR and GEIA data sets proved to be very close, although total emissions for 1990 increased from the amount estimated for 1985 using the same approach.

3.2. Projection of the Evolution of Urban Areas

The procedure used above to derive the geographical distribution and PDFs of urban emissions is based on existing emissions inventories and cannot automatically be used for future projections. We adopted a reasonable approach to project the spatial patterns of urban emissions, based on predictions of total emissions and energy consumption by the EPPA model and urban population projections of the United Nations (UN), under the assumption that PDFs of pollutant emissions do not change over time. The latter assumption

Table 4. Projections of the Percentage of the Population Living in Urban Areas (pop_{urb}) for Several EPPA Regions Through the Year 2100[a]

Pop_{urb}, %	1990	2000	2020	2040	2060	2080	2100
world	43.2	47.4	56.7	65.6	69.9	72.7	74.5
USA	75.2	77.2	82.2	85.5	85.2	85.4	85.2
JPN	77.4	78.9	83.2	86.2	87.6	88.7	90.3
EEC	77.8	79.3	83.6	86.6	87.7	88.3	88.4
OOE	70.2	76.8	83.8	86.4	87.3	87.4	87
EET	58.5	62.6	71.0	77.6	81.2	83.3	83.9
FSU	68.5	76.5	75.8	82.8	84.0	86.8	88.9
EEX	48.6	55.8	67.1	74.3	76.0	77.0	77.8
CHN	26.2	34.3	49.1	57.9	59.4	59.3	58.9
IND	25.2	28.4	39.2	53.1	59.8	63.2	65.2
DAE	47.7	55.7	65.3	72.8	77.2	78.9	79.9
BRA	74.7	81.3	87.3	89.6	91.3	92.1	92.6
ROW	43.2	47.4	56.7	65.6	69.9	72.7	74.5

[a] Projections from *United Nations* [1992, 1998]. The greatest increase is projected for non-Annex B countries or regions such as China, India, DAE, and EEX. Abbreviations are EEC: United Kingdom, Ireland, France, Germany, Netherlands, Belgium, Luxembourg, Spain, Portugal, Italy, Greece, Denmark; OOE: Australia, Canada, New Zealand, Turkey, Austria, Sweden, Finland, Norway; EET: Bulgaria, Czechoslovakia, Hungary, Poland, Romania, Yugoslavia; EEX: Iran, Iraq, Kuwait, Saudi Arabia, Venezuela, Qatar, Indonesia, Libya, United Arab Emirates, Algeria, Nigeria, Ecuador, Gabon, Mexico; DAE: Hong Kong, Philippines, Singapore, South Korea, Taiwan, Thailand; ROW: Rest of the world; FSU: Former Soviet Union.

Table 5. Urban NO_x Emissions, Urban Population, and Energy Consumption per Capita for Several EPPA Regions in 1990[a]

	USA	EEC	Japan	FSU	India	China	Brazil
Urban NO_x, EDGAR, Tg N/yr	5.03	2.58	0.576	1.125	0.156	1.1	0.145
Urban population, thousands	186,835	272,463	95,040	189,895	230,269	380,803	112,643
Energy/capita, EPPA, GJ/person	311.9	141.2	137.4	186.1	10.49	33.06	15.34
α, ng/J	86.2	67.0	44.1	32.0	64.7	87.4	83.9

[a] The coefficient α is calculated using (1).

assumes that at a sufficiently high level of emissions, pollution regulations will be established to limit these emissions, as is the case in most of the developed world.

The UN population projections [*United Nations*, 1992, 1998] suggest a worldwide increase in urban population over the upcoming decades. Within the next 10 years the number of urban dwellers is expected to exceed the number of people living in rural areas. Figure 2 shows projections of the urban population for several EPPA regions based on the above UN data for the next century. The percentages of the population living in urban areas in the world and in each EPPA region from 1990 through 2100 are listed in Table 4.

As noted earlier, urban areas are differentiated from nonurban areas by their high NO_x emissions. To estimate future urban NO_x emissions, we link NO_x emissions to the urban population. We assume that the amount of NO_x emitted from cities is proportional to the product of urban population and energy consumption per capita, which is predicted by the EPPA model. We can then formulate the following equation for urban NO_x emissions ($NO_{x(\text{urban})}$) for each EPPA region:

$$NO_{x(\text{urban})} = E_C P_{\text{urban}} \alpha , \quad (1)$$

where E_C is the regional energy consumption per capita, P_{urban} is the total urban population in the region, and α is a constant of proportionality that does not change over time. The constant α was determined for several EPPA regions for 1990 by deriving $NO_{x(\text{urban})}$ from the EDGAR inventory, E_C from the EPPA model, and P_{urban} from UN statistics. Table 5 lists the values of α for several EPPA regions. For our calculations of future urban NO_x emissions, an α value of 66 ng/J was used, where α is the arithmetic mean of the α variables calculated for several EPPA regions. Note that this approach does not permit the inclusion of technology changes, such as catalysts or other energy efficiency advances, which could reduce emissions per unit of energy consumption.

A different approach was adopted to project urban CO and NMVOC emissions. The two main anthropogenic sources of CO emissions are fossil fuel combustion and biomass burning, and this is reflected in the EDGAR 2.0 inventory for 1990 [*Olivier et al.*, 1995]. Economic development in any given region changes the relative importance of these two sources. Fossil fuel combustion increases with development, while biomass burning decreases and can eventually almost disappear in highly developed regions such as the United States [*U.S. Environmental Protection Agency*, 1997]. This behavior is reflected in the ratio of the percentage of urban NO_x emissions ($NO_{x\%}$) to the percentage of urban CO emissions ($CO_{\%}$): high percentages of both urban NO_x and urban CO emissions implies a highly developed economy. Figure 3 plots the ratio of $NO_{x\%}$ to $CO_{\%}$ against $NO_{x\%}$. Data for the graph were derived from the EDGAR inventory for 1990 at several latitudinal bands in the Southern and Northern Hemispheres, each of which contains more than three urban areas. The quadratic fit of $NO_{x\%}/CO_{\%}$ to $NO_{x\%}$ yields the following relationship that can be used to calculate future urban CO emissions:

$$CO_{\%}(t) = \frac{NO_{x\%}(t)}{3.08 - 0.02 \cdot NO_{x\%}(t) - 2.64 \cdot (NO_{x\%}(t))^2} . \quad (2)$$

Here t is time and $NO_{x\%}(t)$ is calculated using (1).

Since NMVOC emissions are not projected by the EPPA model, the following approximation to forecast NMVOC emissions (E_{VOC}) based on CO emissions was developed:

$$E_{\text{VOC}} = (1 + \text{DVOC})(0.2E_{\text{CO}} + 0.98) . \quad (3)$$

Here E_{CO} represents CO emissions (in kg C/km^2 d), which have the PDF shown in Figure 1a, and DVOC is the deviation from the PDF of the CO emissions. DVOC itself is assumed to have a normal distribution, with a mean value of 0.47 kg/(km^2 d) and a standard deviation (σ) of 0.23. The percentages of urban SO_x emissions are always the 1990 values.

As urban populations increase, more urban areas that are highly polluted can be expected. The amount of urban NO_x emissions in each latitudinal band serves as a base for calculating the number of urban areas in years other than 1990. Assuming that the PDFs of urban NO_x, SO_x, CO, and NMVOC emissions do not change, we can determine the average NO_x emissions E_0 from urban areas in 1990 based on

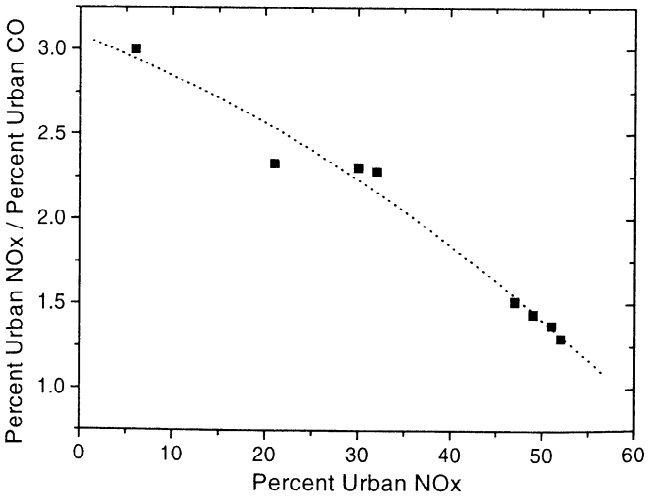

Figure 3. The ratio of urban NO_x to urban CO emissions versus the percentage of urban NO_x emissions. The dotted line is a quadratic fit to the data that were derived from the EDGAR 2.0 1990 database.

the EDGAR inventory. Given a city of size 200 km x 200 km, E_0 has the value 4 x 10^5 kg N/d. The number of urban areas N in each latitudinal band is then given by the equation

$$N = \frac{E_{\text{total}}}{E_0}, \tag{4}$$

where E_{total} is the total amount of emissions predicted for the relevant latitudinal band, in kg/d.

3.3. Urban Airshed Model

Our parameterization of urban atmospheric chemistry is based on the California Institute of Technology–Carnegie Institute of Technology (at Carnegie Mellon University) Urban Airshed Model, hereinafter referred to as the CIT Model [*McRae et al.*, 1982]. The CIT Model solves numerically the atmospheric chemical continuity equation:

$$\frac{\partial C_i}{\partial t} + \nabla \cdot (\vec{u} C_i) = \nabla \cdot (\mathbf{K} \nabla C_i) + R_i + Q_i, \tag{5}$$

where C_i is the ensemble mean concentration (mole/volume) of a given species i, $\vec{u}$ is the wind velocity, $\mathbf{K}$ is the eddy diffusivity matrix, R_i is the chemical production rate of species i, and Q_i is the source term for elevated point sources of species i. The surface boundary condition is given by the following equation:

$$-K_{zz} \frac{\partial C_i}{\partial z} = E_i - v_g^i C_i. \tag{6}$$

The upward flux of each pollutant equals direct emissions subtracted from the dry deposition flux. The vertical eddy diffusivity is K_{zz}, E_i is the ground-level emission flux, and v_g^i is the dry deposition velocity for species i [*McRae et al.*, 1982].

The chemical formulation used in the CIT Model is a modification of the condensed Lurmann-Carter-Coyner formulation [*Lurmann et al.*, 1987a,b; *Harley et al.*, 1993] and includes 35 differential and 9 steady state chemical species (see Table 6). The isoprene coefficients have not been updated since *Carter* [1990]; the present study's simulations did not include isoprene emissions. Nine lumped organic classes represent more than 100 organic species. The 106 reactions in the mechanism include 34 inorganic reactions, all listed in Table 6. Photolysis reactions of all the following are included: NO_2, NO_3 (two channels), O_3 (two channels), HONO, HCHO (two channels), ALD (acetaldehyde), MEK (methyl ethyl ketone), MGLY (methyl glyoxal), and DIAL (dicarbonyls). The lumping is typically done on a per mole basis. Some product coefficients are determined by key characteristics of the lumped classes (such as the fraction of terminal alkenes, or the fraction of trisubstituted aromatics). The CIT Model version used in this study has been tested against observational data gathered during the 1987 Southern California Air Quality Study [*Harley et al.*, 1993].

3.4. Reduced-Form Model for Urban Atmospheric Chemical Processes

To derive the reduced form of the CIT Model, we employed the probabilistic collocation method [*Tatang et al.*, 1997] (sometimes called the deterministic equivalent modeling method). This method approximates a model's response to uncertain inputs by orthogonal polynomial functions in a chaos expansion. For each output variable a separate reduced-form model is developed. Compared to traditional statistical methods such as the Monte Carlo method, the probabilistic collocation method appears to be computationally inexpensive for complex models that are not highly nonlinear. *Calbo et al.* [1998] showed that the probabilistic collocation method yields reduced forms that closely approximate the CIT Model.

In this study, urban atmospheric chemistry is parameterized in a 200 km x 200 km urban area with a height of 2.09 km. The model domain has five vertical layers with heights (from the lowest layer to the highest) of 73, 293, 585, 1275, and 2090 m. The total integration time is 24 hours.

We restrict the total number of input parameters to 15: date; latitude; wind speed; temperature; cloudiness; mixing layer height; emissions of NO_x, SO_2, CO, and NMVOC; and initial and boundary conditions for NO, NO_2, ozone, SO_2, and NMVOC (the latter expressed using an air quality index (AQI) as defined by *Calbo et al.* [1998]). For several parameters such as temperature, wind speed, mixing layer height, and several chemical emission rates, daily cycles are assumed [*Calbo et al.*, 1998]. Air temperature is assumed to oscillate ±4°C around the input temperature (daily mean temperature) with the minimum at sunrise, the maximum at 1400 LT, and linear variations in between. The mixing layer height is equal to the maximum mixing layer height, which is an input value, between 1400 LT and sunset. Between 2 hours after sunset and sunrise the model's mixing layer height is set to its nighttime value, 20 times smaller than the maximum or 50 m, whichever is higher. The value of the mixing layer height is linearly interpolated for the time period between the maximum and minimum values. No spatial variations are assumed for the temperature and mixing layer height fields.

Emission fields of NO_x, CO, and NMVOC (we assume no diurnal variation in SO_2 emissions) have the same daily cycle in addition to their spatial emission patterns. Emissions are assumed to be high during the day (0600–1800 LT) with a maximum at 1500 LT and low at night (roughly 4 times lower than daytime values). For more details, see *Calbo* et al. [1998]. Surface emissions, applied in the model to a circular area with a diameter of 150 km, are assumed to be highest in the center (at which point the emissions strength is assumed to be 8 times the defined input emissions strength), decreasing gradually toward the perimeter (where the emissions strength is assumed to be 0.1 times the defined input emissions strength). We assume further that air entering the modeling domain is clean and has trace species concentrations typical for remote areas. The 58 model outputs can be summarized in three sets, namely, (1) the total aggregated fluxes in a 24-hour period of NO, NO_2, O_3, HCHO, peroxy-acetyl nitrate (PAN), N_2O_5, HONO, HNO_3, CO, SO_2, and SO_3 from the urban modeling domain; (2) the moles of NO, NO_2, O_3, HCHO, CO, SO_2, SO_3, and several lumped hydrocarbon species such as ALD2, MEK, ALKA, ETHE, ALKE, TOLU, and AROM (Table 7 defines these acronyms) inside the model domain after a 24-hour simulation; and (3) the daily average moles of all 31 species considered in this study (i.e., the first 31 CIT species listed in Table 6). The total aggregated net flux over 24 hours is defined as

$$\text{flux}_{\text{total}}^i = \text{flux}_{\text{out}}^i - \text{flux}_{\text{in}}^i - \text{depo}_i + \text{emiss}_i, \tag{7}$$

where $\text{flux}_{\text{out}}^i$ is the aggregated flux of species i out of the

Table 6. Gas Phase Chemical Reactions Included in the CIT Model[a]

Number	Reaction	Rate Constant	References
(R1)	$NO_2 + h\nu \rightarrow NO + O$	radiation dependent	1
(R2)	$O + O_2 + M \rightarrow O_3 + M$	$1.05 \times 10^{4}\ e^{1282/T}$	1
(R3)	$O + NO_2 \rightarrow NO + O_2$	9.3×10^{-12}	1
(R4)	$O + NO_2 + M \rightarrow NO_3 + M$	$1.11 \times 10^{-13}\ e^{894/T}$	1
(R5)	$NO + O_3 \rightarrow NO_2$	$1.8 \times 10^{-12}\ e^{-1370/T}$	1
(R6)	$NO_2 + O_3 \rightarrow NO_3$	$1.2 \times 10^{-13}\ e^{-2450/T}$	1
(R7)	$NO + NO_3 \rightarrow 2\ NO_2$	$8 \times 10^{-12}\ e^{252/T}$	1
(R8)	$NO + NO \rightarrow 2\ NO_2$	$1.64 \times 10^{-20}\ e^{529/T}$	1
(R9)	$NO_2 + NO_3 + M \rightarrow N_2O_5 + M$	$4.62 \times 10^{-13}\ e^{273/T}$	1
(R10)	$N_2O_5 \rightarrow NO_2 + NO_3$	$1.33 \times 10^{15}\ e^{-11379/T}$	1
(R11)	$N_2O_5 + H_2O \rightarrow 2\ HNO_3$	1×10^{21}	1
(R12)	$NO_2 + NO_3 \rightarrow NO + NO_2$	$2.5 \times 10^{-14}\ e^{-1229/T}$	1
(R13)	$NO_3 + h\nu \rightarrow NO$	radiation dependent	1
(R14)	$NO_3 + h\nu \rightarrow NO_2 + O$	radiation dependent	1
(R15)	$O_3 + h\nu \rightarrow O$	radiation dependent	1
(R16)	$O_3 + h\nu \rightarrow OSD$	radiation dependent	1
(R17)	$OSD + H_2O \rightarrow 2\ OH$	2.2×10^{-10}	1
(R18)	$OSD \rightarrow O$	7.2×10^{8}	1
(R19)	$NO + OH + M \rightarrow HONO + M$	$4.03 \times 10^{-13}\ e^{833/T}$	1
(R20)	$HONO + h\nu \rightarrow NO + OH$	radiation dependent	1
(R21)	$NO_2 + H_2O \rightarrow HONO - NO_2 + HNO_3$	4×10^{-24}	1
(R22)	$NO_2 + OH + M \rightarrow HNO_3 + M$	$9.58 \times 10^{-13}\ e^{737/T}$	1
(R23)	$HNO_3 + OH \rightarrow NO_3$	$9.4 \times 10^{-15}\ e^{778/T}$	1
(R24)	$CO + OH \rightarrow HO_2$	2.18×10^{-13}	1
(R25)	$O_3 + OH \rightarrow HO_2$	$1.6 \times 10^{-12}\ e^{-942/T}$	1
(R26)	$NO + HO_2 \rightarrow NO_2 + OH$	$3.7 \times 10^{-12}\ e^{240/T}$	1
(R27)	$NO_2 + HO_2 \rightarrow HNO_4$	$1.02 \times 10^{-13}\ e^{773/T}$	1
(R28)	$HNO_4 \rightarrow NO_2 + HO_2$	$4.35 \times 10^{13}\ e^{-10103/T}$	1
(R29)	$HNO_4 + OH \rightarrow NO_2$	4×10^{-12}	1
(R30)	$O_3 + HO_2 \rightarrow OH$	$1.4 \times 10^{-14}\ e^{-579/T}$	1
(R31)	$HO_2 + HO_2 \rightarrow H_2O_2$	$2.27 \times 10^{-13}\ e^{771/T}$	1
(R32)	$HO_2 + HO_2 + H_2O \rightarrow H_2O_2$	$3.26 \times 10^{-34}\ e^{2971/T}$	1
(R33)	$NO_3 + HO_2 \rightarrow HNO_3$	$2.27 \times 10^{-13}\ e^{771/T}$	1
(R34)	$NO_3 + HO_2 + H_2O \rightarrow HNO_3$	$3.26 \times 10^{-34}\ e^{2971/T}$	1
(R35)	$RO_2 + NO \rightarrow NO$	$4.2 \times 10^{-12}\ e^{180/T}$	1
(R36)	$RO_2 + HO_2 \rightarrow HO_2$	3×10^{-12}	1
(R37)	$RO_2 + RO_2 \rightarrow$ products	1×10^{-15}	1
(R38)	$RO_2 + MCO_3 \rightarrow$ products	3×10^{-12}	1
(R39)	$HCHO + h\nu \rightarrow 2\ HO_2 + CO$	radiation dependent	1
(R40)	$HCHO + h\nu \rightarrow CO$	radiation dependent	1
(R41)	$HCHO + OH \rightarrow HO_2 + CO$	9×10^{-12}	1
(R42)	$HCHO + NO_3 \rightarrow HNO_3 + HO_2 + CO$	$6 \times 10^{-13}\ e^{-2060/T}$	1
(R43)	$HCHO + HO_2 \rightarrow RO_2R + RO_2$	1×10^{-14}	1
(R44)	$ALD2 + OH \rightarrow MCO_3$	$6.9 \times 10^{-12}\ e^{250/T}$	1
(R45)	$ALD2 + h\nu \rightarrow CO + HCHO + RO_2R + HO_2C + RO_2$	radiation dependent	1
(R46)	$ALD2 + NO_3 \rightarrow HNO_3 + MCO_3$	$3 \times 10^{-13}\ e^{-1427/T}$	1
(R47)	$MCO_3 + NO \rightarrow NO_2 + HCHO + RO_2R + RO_2$	$4.2 \times 10^{-12}\ e^{180/T}$	1
(R48)	$MCO_3 + NO_2 \rightarrow PAN$	$2.8 \times 10^{-12}\ e^{180/T}$	1
(R49)	$MCO_3 + HO_2 \rightarrow HCHO$	3×10^{-12}	1
(R50)	$MCO_3 + MCO_3 \rightarrow 2\ HO_2 + 2\ HCHO$	2.5×10^{-12}	1
(R51)	$PAN \rightarrow MCO_3 + NO_2$	$2 \times 10^{16}\ e^{-13542/T}$	1
(R52)	$MEK + h\nu \rightarrow MCO_3 + ALD2 + RO_2R + RO_2$	radiation dependent	1
(R53)	$MEK + OH \rightarrow 1.2\ R_2O_2 + 1.2\ RO_2 + MCO_3 + 0.5\ ALD2 + 0.5\ HCHO$	$1.2 \times 10^{-11}\ e^{-745/T}$	1
(R54)	$MGLY + h\nu \rightarrow MCO_3 + HO_2 + CO$	radiation dependent	1
(R55)	$MGLY + OH \rightarrow MCO_3 + CO$	1.7×10^{-11}	1
(R56)	$MGLY + NO_3 \rightarrow HNO_3 + MCO_3 + CO$	$3 \times 10^{-13}\ e^{-1427/T}$	1
(R57)	$ALKA + OH \rightarrow B1\ HCHO + B2\ ALD2 + B3\ MEK + B4\ RO_2N + B6\ R_2O_2 + B7\ RO_2$	$1.053 \times 10^{-11}\ e^{-354/T}\ X + 1.62 \times 10^{-11}\ e^{-289/T}(1-X)$	1[b,c]
(R58)	$ALKN + OH \rightarrow NO_2 + 0.15\ MEK + 1.53\ ALD2 + 0.16\ HCHO + 1.39\ R_2O_2 + 1.39\ RO_2$	$2.19 \times 10^{-11}\ e^{-709/T}$	1
(R59)	$RO_2N + NO \rightarrow ALKN$	$4.2 \times 10^{-12}\ e^{180/T}$	1

Table 6. (continued)

Number	Reaction	Rate Constant	References
(R60)	$RO_2N + HO_2 \rightarrow$ MEK	3×10^{-12}	1
(R61)	$RO_2N + RO_2 \rightarrow RO_2 + HO_2 +$ MEK	1×10^{-15}	1
(R62)	$RO_2N + MCO_3 \rightarrow$ HCHO + HO_2 + MEK	3×10^{-12}	1
(R63)	$R_2O_2 + NO \rightarrow NO_2$	$4.2 \times 10^{-12} e^{180/T}$	1
(R64)	$R_2O_2 + HO_2 \rightarrow$ products	3×10^{-12}	1
(R65)	$R_2O_2 + RO_2 \rightarrow RO_2$	1×10^{-15}	1
(R66)	$R_2O_2 + MCO_3 \rightarrow$ HCHO + HO_2	3×10^{-12}	1
(R67)	$RO_2R + NO \rightarrow NO_2 + HO_2$	$4.2 \times 10^{-12} e^{180/T}$	1
(R68)	$RO_2R + HO_2 \rightarrow$ products	3×10^{-12}	1
(R69)	$RO_2R + RO_2 \rightarrow 0.5\ HO_2$ + RO2	1×10^{-15}	1
(R70)	$RO_2R + MCO_3 \rightarrow HO_2$ + HCHO	3×10^{-12}	1
(R71)	ETHE + OH $\rightarrow RO_2R + RO_2$ + 1.56 HCHO + 0.22 ALD2	$2.15 \times 10^{-12} e^{411/T}$	1
(R72)	ETHE + $O_3 \rightarrow$ HCHO + 0.12 HO_2 + 0.42 CO	$1.2 \times 10^{-14} e^{-2634/T}$	1
(R73)	ETHE + O $\rightarrow RO_2R + RO_2$ + CO + HCHO + HO_2	$1.04 \times 10^{-11} e^{-792/T}$	1
(R74)	ETHE + $NO_3 \rightarrow RO_2 + NO_2$ + 2 HCHO + R_2O_2	$2 \times 10^{-12} e^{-2925/T}$	1
(R75)	ALKE + OH $\rightarrow RO_2 + RO_2$ + *B8* HCHO + *B9* ALD2	$4.85 \times 10^{-12} e^{504/T} Y + 1.01 \times 10^{-11} e^{549/T} (1\text{-}Y)$	1[b,d]
(R76)	ALKE + $O_3 \rightarrow$ *B10* HCHO + *B11* ALD2 + *B12* RO_2R + *B12* RO_2 + *B13* HO_2 + *B14* OH + *B15* CO	$1.32 \times 10^{-4} e^{-2105/T} Y + 9.08 \times 10^{-15} e^{-1137/T} (1\text{-}Y)$	1[b,d]
(R77)	ALKE + O $\rightarrow$ *B16* CO + *B17* MEK + *B18* HCHO + *B19* ALD2 + *B20* HO_2 + *B21* RO_2R + *B21* RO_2	$1.18 \times 10^{-11} e^{-324/T} Y + 2.26 \times 10^{-11} e^{10/T} (1\text{-}Y)$	1[b,d]
(R78)	ALKE + $NO_3 \rightarrow NO_2$ + *B8* HCHO + *B9* ALD2 + $R_2O_2 + RO_2$	$5 \times 10^{-12} e^{-1935/T} + 1 \times 10^{-11} e^{-975/T} (1\text{-}Y)$	1[b,d]
(R79)	TOLU + OH $\rightarrow$ 0.16(CRES + HO_2) + 0.4 DIAL + 0.84 RO_2 + 0.144 MGLY + 0.11 HCHO + 0.114 CO + 0.84 RO_2R	$2.1 \times 10^{-12} e^{322/T}$	1
(R80)	AROM + OH $\rightarrow$ 0.17 CRES + 0.17 HO_2 + 0.83 RO_2R + 0.83 RO_2 + *B22* DIAL + *B23* MGLY + *B24* CO	$1.66 \times 10^{-11} e^{116/T} Z + 6.2 \times 10^{-11} (1\text{-}Z)$	1[b,e]
(R81)	DIAL + OH $\rightarrow MCO_3$	3×10^{-11}	1
(R82)	DIAL + $h\nu \rightarrow HO_2$ + CO + MCO_3	radiation dependent	1
(R83)	CRES + OH $\rightarrow$ 0.2 MGLY + 0.15 RO_2P + 0.85 $RO_2R + RO_2$	4×10^{-11}	1
(R84)	CRES + $NO_3 \rightarrow HNO_3$ + BZO	2.2×10^{-11}	1
(R85)	RO_2P + NO $\rightarrow$ NPHE	$4.2 \times 10^{-12} e^{180/T}$	1
(R86)	$RO_2P + HO_2 \rightarrow$ products	3×10^{-12}	1
(R87)	$RO_2P + RO_2 \rightarrow 0.5\ HO_2 + RO_2$	1×10^{-15}	1
(R88)	$RO_2P + MCO_3 \rightarrow$ HCHO + HO_2	3×10^{-12}	1
(R89)	BZO + $NO_2 \rightarrow$ NPHE	1.5×10^{-11}	1
(R90)	BZO + $HO_2 \rightarrow$ products	3×10^{-12}	1
(R91)	BZO $\rightarrow$ products	1×10^{-3}	1
(R92)	NPHE + $NO_3 \rightarrow HNO_3 + BZN_2$	3.8×10^{-12}	1
(R93)	$BZN_2 + NO_2 \rightarrow$ products	1.5×10^{-11}	1
(R94)	BZN_2 + HO2 $\rightarrow$ NPHE	3×10^{-12}	1
(R95)	$BZN_2 \rightarrow$ NPHE	1×10^{-3}	1
(R96)	$H_2O_2 + h\nu \rightarrow 2$ OH	radiation dependent	1[f]
(R97)	H_2O_2 + OH $\rightarrow HO_2$	$3.1 \times 10^{-12} e^{-187/T}$	1[f]
(R98)	MEOH + OH $\rightarrow$ HCHO + HO_2	$5.75 \times 10^{-13} T^2 e^{148/T}$	2
(R99)	CH_4 + OH $\rightarrow$ HCHO + $RO_2 + RO_2R$	$6.95 \times 10^{-18} T^2 e^{-1282/T}$	2
(R100)	ISOP + OH $\rightarrow$ HCHO + ALD2 + $RO_2R + RO_2$	$2.54 \times 10^{-11} e^{410/T}$	2
(R101)	ISOP + $O_3 \rightarrow$ 0.5 HCHO + 0.65 ALD2 + 0.21 MEK + 0.16 HO_2 + 0.29 CO + 0.06 OH + 0.14 ($RO_2R + RO_2$)	$1.23 \times 10^{-14} e^{-2013/T}$	2
(R102)	ISOP + O $\rightarrow$ 0.4 HO_2 + 0.5 MEK + 0.5 ALD2	6×10^{-11}	2
(R103)	ISOP + $NO_3 \rightarrow NO_2$ + HCHO + ALD2 + $R_2O_2 + RO_2$	$2.54 \times 10^{-11} e^{-1121/T}$	2
(R104)	ETOH + OH $\rightarrow$ ALD2 + HO_2	$5.56 \times 10^{-13} T^2 e^{532/T}$	2
(R105)	MTBE + 1.4 OH $\rightarrow$ 0.6 TBF + 0.4 HCHO + 0.4 MEK + 1.4 RO_2R + 0.4 R_2O_2 + 1.8 RO_2	$6.82 \times 10^{-18} T^2 e^{460/T}$	3, 4
(R106)	SO_2 + OH $\rightarrow SO_3 + HO_2$	9.1×10^{-13}	2

[a] from *Lurmann et al.* [1987a,b]; Rate constants given in cm^3 $molecule^{-1}$ s^{-1}; T in Kelvin. References are 1, *Lurmann et al.* [1987a, b], condensed Lurmann-Carter-Coyner (LCC) mechanism; 2, *Carter* [1990]; 3, *Japar et al.* [1990]; 4, *Atkinson* [1990].

[b] B_i in (R57), (R75), (R76), (R77), (R78), and (R80) are pressure- and temperature-dependent stochiometric coefficients of the condensed LCC mechanism; for details, see *Lurmann et al.* [1987a, b].

[c] X is the ratio of C4-C5 alkanes to > C3 alkanes on a mole basis; see *Lurmann et al.* [1987a, b].

[d] Y is the ratio of terminal alkenes to > C2 alkenes on a mole basis; see *Lurmann et al.* [1987a, b].

[e] Z is the ratio of di-alkylbenzenes to di- and tri-alkylbenzenes on a mole basis; see *Lurmann et al.* [1987a, b].

[f] OZIPM mechanism is another condensed mechanism of the LCC formulation intended for use in Ozone Isopleth Plotting Package with Optional mechanisms (OZIPM); see *Lurmann et al.* [1987a, b].

Table 7. CIT Species Definitions

Abbreviation	Species Name
NO	nitric oxide
NO_2	nitrogen dioxide
O_3	ozone
HONO	nitrous acid
HNO_3	nitric acid
HNO_4	pernitric acid
N_2O_5	nitrogen pentoxide
NO_3	nitrate radical
HO_2	hydroperoxy radical
CO	carbon monoxide
HCHO	formaldehyde
ALD2	lumped aldehydes
MEK	methyl ethyl ketone
MGLY	methylglyoxyl
PAN	Peroxyl-acetyl nitrate
RO_2	total RO_2 radicals
MCO_3	CH_3CO_3 radical
ALKN	alkyl nitrate
ALKA	>C3 alkanes
ETHE	ethene
ALKE	>C2 alkenes
TOLU	toluene
AROM	aromatics
DIAL	unknown dicarbonyls
NPHE	nitrophenols
NH3	ammonia
NIT	aerosol nitrate
MEOH	methanol
ETOH	ethanol
MTBE	methyl tert-butyl ether
OSD	O singlet D
O	O atom
OH	hydroxyl radical
RO_2R	general RO_2 #1
R_2O_2	general RO_2 #2
RO_2N	alkyl nitrate RO_2
RO_2P	phenol RO_2
BZN2	benzaldehyde N-RO_2
BZO	phenoxy radical
ISOP	isoprene
H_2O_2	hydrogen peroxide
H_2O	water vapor
O_2	oxygen
H_2	hydrogen
SO_2	sulfur dioxide
SO_3	sulfur trioxide
M	third body
TBF	tert-butyl formate, treated as inert species

domain, $\text{flux}_{\text{in}}^{i}$ is the aggregated flux of species i into the domain, depo_i is the aggregated dry deposition flux of species i, and emiss_i represents the aggregated emissions of species i. The aggregated fluxes give the effective emissions from urban areas into the global 2D-LO model grid. At the end of each 24-hour simulation, the moles of several species are used to initialize the reduced-form models for the next day's runs and to determine mole fractions at 2D-LO model grid points. Besides moles and fluxes, a variable referring to the maximum ozone mole fraction in the model domain is also computed. This variable (the same as that given by *Calbo et al.* [1998]) is defined as the surface domain average O_3 mole fraction at the time the absolute surface peak O_3 occurs. The value of this maximum ozone mole fraction is typically a factor of 2 to 5 times higher than the domain average O_3 mole fraction. The reduced-form urban model is designed to approximate the CIT predictions of 24-hour integrated fluxes out of the urban modeling domain and total moles in the urban modeling domain at the end of the 24-hour simulation (i.e., midnight). Therefore it does not explicitly predict the diurnal variations, though these are fully included in the calculations of the integrated fluxes.

We chose a third-order polynomial chaos expansion including relevant cross terms to obtain the reduced-form model (*Calbo et al.* [1998] had done a second-order polynomial chaos expansion). The seasonal dependence of the output variables is expressed as

$$y_i = y_0^i + \frac{y_0^i}{C_i}\sin\left(\frac{\pi(x - x_c^i)}{w_i}\right), \tag{8}$$

where y_0^i is the output from the reduced-form model; C_i is a constant determined by fitting CIT Model data, and relates to the amplitude of the sine function for output i; x is the Julian day; x_c^i gives the phase of the cycle; and w_i is the period (12 months).

The present study used normal distributions (Figure 1) for the PDFs of emissions instead of the beta distributions used by *Calbo et al.* [1998] because the global emissions inventory data could be fitted best with normal distributions. We also used the global emissions inventories to derive the PDF of each pollutant separately. This approach should provide more accurate results and more reasonable coverage of the emissions range than the previous study, which employed only a small data set and assumed constant proportionalities (1) between CO and NMVOC emissions and (2) between CO and NO_x emissions [*Calbo et al.*, 1998]. As a result, our NO_x emissions range from 0 to 60 kg N/(km^2 d) with a mean of 6 kg N/(km^2 d), whereas *Calbo et al.* [1998] defined a range from 0 to 115 kg N/(km^2 d) with a mean of 23 kg N/(km^2 d). The CO range is the same in both studies (0 to 500 kg C/(km^2 d)) but our mean value of 50 kg C/(km^2 d) is half the value used by *Calbo et al.* [1998]. The new NMVOC emissions range from 0 to 350 kg NMVOC/(km^2 d) with a mean of 22 kg NMVOC/(km^2 d) contrasts with that obtained by *Calbo et al.* [1998]: 0 to 160 kg NMVOC/(km^2 d) with a mean of 33 kg NMVOC/(km^2 d). Finally, our SO_2 emissions were assumed to be between 0 and 330 kg S/(km^2 d), compared to *Calbo et al.* [1998]'s range of 0 to 50 kg S/(km^2 d), but both studies derived the same mean, 11 kg S/(km^2 d).

Another major improvement this study offers over that conducted by *Calbo et al.* [1998] regards the initial profiles of pollutants: *Calbo et al.* [1998] assumed that pollutants at the beginning of each model day exist only in the first two model layers. The present study's profiles include all five model layers. This modification is important especially for species like ozone and CO because the boundary conditions determine also the incoming flux into the urban domain. This change in the initial profiles most affects ozone production and related processes such as the formation of PAN.

Results of the reduced-form model and those of the parent CIT Model are shown for selected outputs in Figures 4a, 4b,

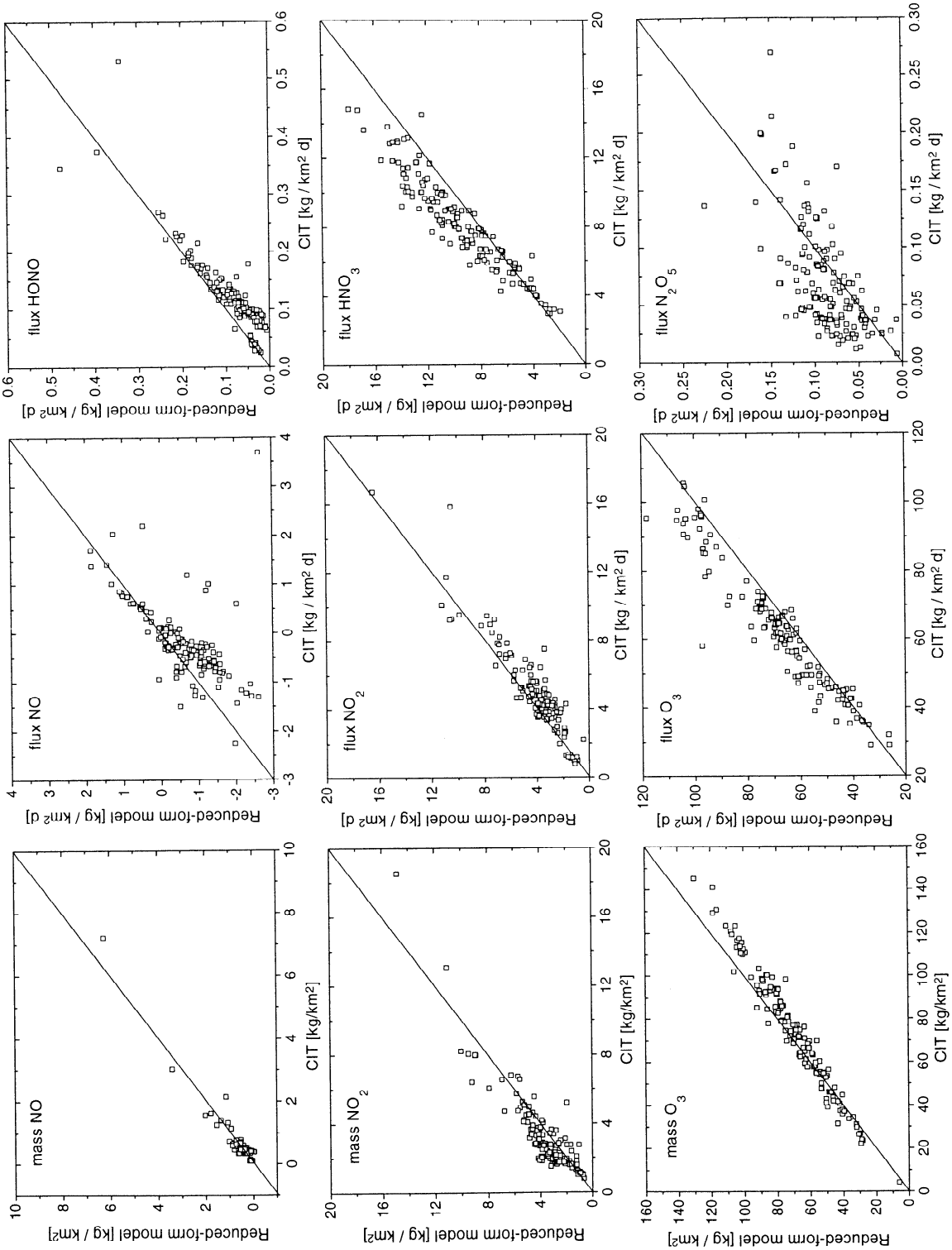

Figure 4a. Comparison between reduced-form urban model results and parent CIT Model results. Input values differ from those used to derive the reduced-form urban model. Fluxes are defined as the total aggregated net mass of emissions per km^2 flowing out of the urban domain during a 24-hour period; masses are the total mass per km^2 in the urban domain at the end of the 24-hour simulation

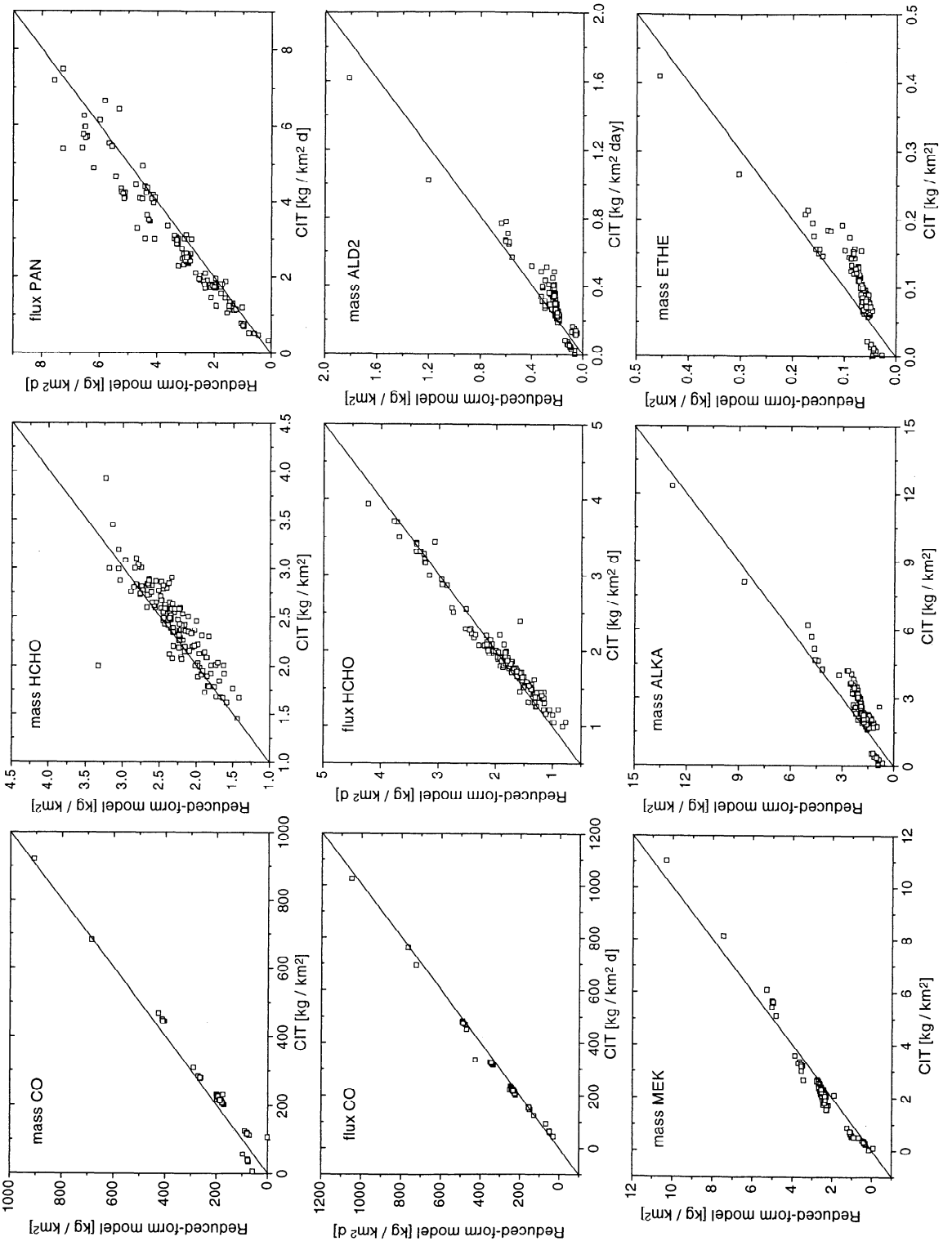

Figure 4b. Comparison between reduced-form urban model results and parent CIT Model results. For species acronyms, see Table 7.

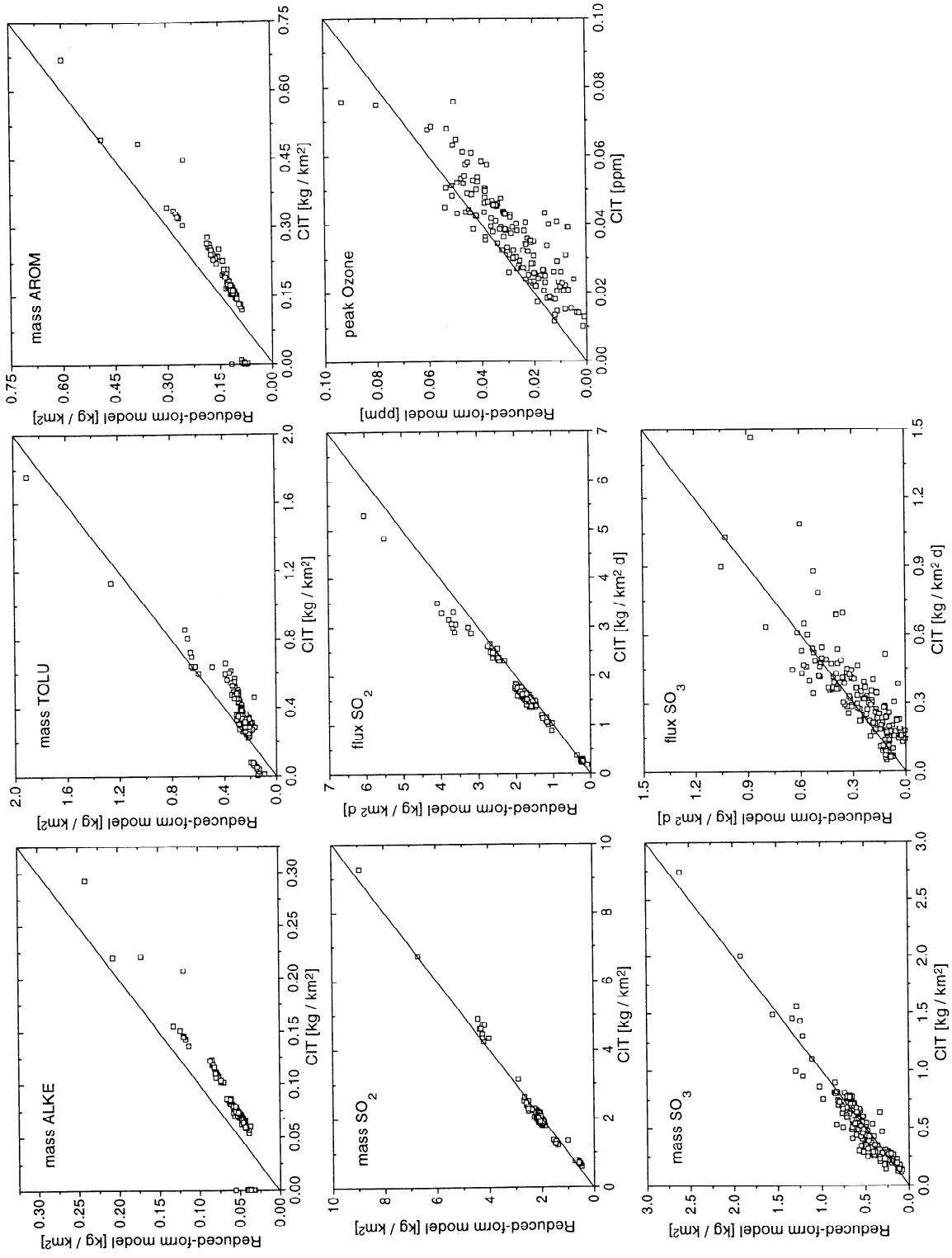

Figure 4c. Comparison between reduced-form urban model results and parent CIT Model results. For species acronyms see Table 7 and for peak ozone definition, see text.

and 4c. The set of input values chosen for the comparison differs from the (collocation) values used to derive the reduced-form model. While the selected testing data cover the whole range of input parameters, the sampling did not reflect exactly the PDFs; however, more points were chosen in the high-probability ranges. All results displayed in Figures 4a, 4b, and 4c are derived for Julian day 181.

Compared to the results of *Calbo et al.* [1998], the reduced-form model's output generally correlates better with the output from the CIT Model. For some species the improvement is obvious (e.g., the flux of CO or PAN in Figure 4b). The two studies' results differ mainly because of changes in the emissions PDFs, but also because the initial vertical profiles of several pollutants differ. Our mean values for the emissions PDFs tend to be lower than the *Calbo et al.* [1998] estimates. In the present study, as well, the peak ozone concentrations substantially exceed the values published by *Calbo et al.* [1998]. This is because new initial vertical profiles of pollutant concentrations (especially of ozone) were introduced. The results of this study are more realistic than the results of *Calbo et al.* [1998], as these new results more closely approximate actual observations.

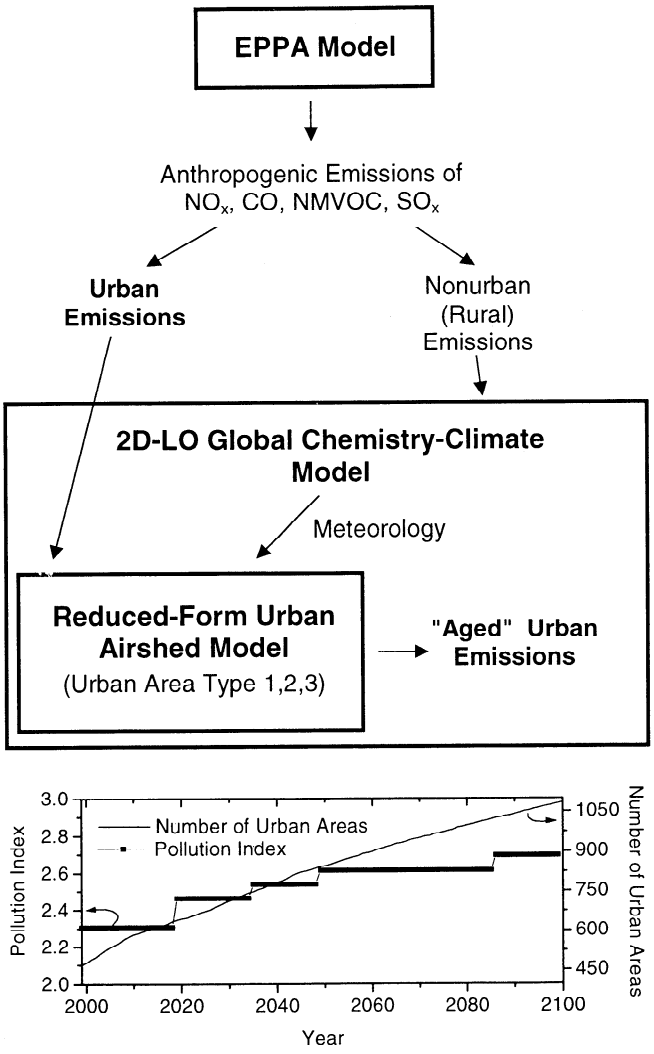

Figure 5. Schematic showing implementation of the reduced-form urban model in the global 2D-LO chemistry-climate model. The bottom graph plots projections for the increase of the number of urban areas and for the change of the pollution index of the urban areas. For detailed description see text.

Table 8. Weighting Coefficients for the Three Types of Urban Areas

Coefficient	Value
γ_1	0.8
γ_2	1.25
γ_3	3.0
γ_4	0.8
γ_5	1.6

4. Linking the Reduced-Form Model With the Global Chemistry-Climate Model

The reduced-form urban atmospheric chemistry model is incorporated into the global interactive 2D-LO chemistry-climate model as a subroutine. Data are communicated between these two every 24 hours. The global model supplies the reduced-form urban models with meteorological data, including wind speeds, temperatures, mixing layer heights, and cloud coverages. The total anthropogenic emissions calculated by the EPPA model are mapped from the EPPA economic regions to the 24 latitudinal bands through use of a population density map [*Fung et al.*, 1991]. The anthropogenic emissions originally input directly into the global model are now separated into urban emissions, which are supplied to the reduced-form models, and rural emissions, which are input to the global model simulations. Figure 5 schematically represents the implementation of the modeling scheme.

In order to save computational time while still representing reasonably cities' different characters with regard to emissions, we assumed three types of urban areas, with low (type 1), medium (type 2), and high (type 3) levels of pollution, respectively. Currently, we assume that the low, medium, and highly polluted cities account for 75%, 20%, and 5%, respectively, of all cities within any latitudinal band. Their emissions can be derived by multiplying the average emissions per urban area E_0 (equation (4)) with a weighting coefficient γ_i. The coefficient γ_i guarantees that the sum of emissions for the three city types equals the total urban emissions. We defined five γ_i. Three (γ_1, γ_2, γ_3) are used for urban area types 1, 2, and 3 when the latitudinal band contains 20 or more polluted cities. Two (γ_4 and γ_5) are used for latitudinal bands with less than 20 but more than 4 urban areas; only low- and medium-polluted cities are assumed. For the latitudinal bands in which fewer than four urban areas are located, only one type is assumed, and emissions are set equal to E_0. Table 8 lists the assumed values for γ_i. Over time we expect relatively more medium and highly polluted urban areas. At the bottom of Figure 5 the predicted increase of urban areas over time is shown in addition to the time development of the global average of a "pollution index" (PI). The PI reflects the number of types of urban areas found in each latitudinal band. It is 1.0 if a band contains only low polluted urban areas (type 1), 2.0 if it contains low and medium polluted urban areas (types 1 and 2), and 3.0 for bands containing all three types of urban areas (types 1, 2, and 3). The global average PI is the arithmetic mean of the PIs of the 13 latitudinal bands for which we allocate urban areas. It

s a step function because we assume three discrete types of ırban areas.

For each latitudinal band of the 2D-LO global model, up to hree urban reduced-form models are executed to provide luxes and moles relevant to the various types of urban areas. The total contribution of urban areas to emissions to be input o the global model and the chemical tracer concentrations to ɔe input at the next iteration of the reduced-form model are hen obtained. First we multiply the fluxes and moles of trace :hemicals for each type of urban area by the total number of ;uch areas within the latitudinal band; second, we sum the ıged emissions or average the mole fractions obtained in the ɔrior step for all three types of urban areas.

After both global and urban models have completed their laily integrations at midnight, the fluxes from the urban nodels are used as emissions to be added to the rural :missions supplied to the global 2D-LO model for its next lay's integration. At the same time the mole fractions of :hemical species at the grid points of the global model in its lowest three layers are updated by combining, with mass-weighting, the total moles of species in both urban and rural ıreas, as predicted by the two models separately, and dividing ɔy the total moles of air in the lowest three layers.

Initial conditions in the urban domains for the next day's ;imulations are set by air quality indices (AQIs) for NO, NO_2, ɔzone, SO_2, and NMVOC, derived using the moles of these ;pecies in the urban domains at the end of the 24-hour simulations. The AQI is a measure of how many moles of a certain species are present in the modeling domain. If we calculate the AQI for a species at the end of a 24-hour simulation, we have a measure of the moles of that species in the modeling domain at the end of our run. Since we assume

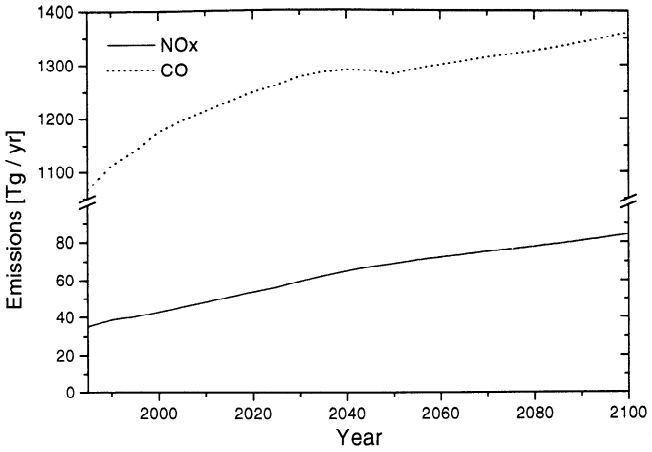

Figure 6. Total anthropogenic NO_x and CO emissions predicted by the economic model (EPPA) from 1985 through 2100, assuming no policy actions are taken to reduce or cap anthropogenic emissions.

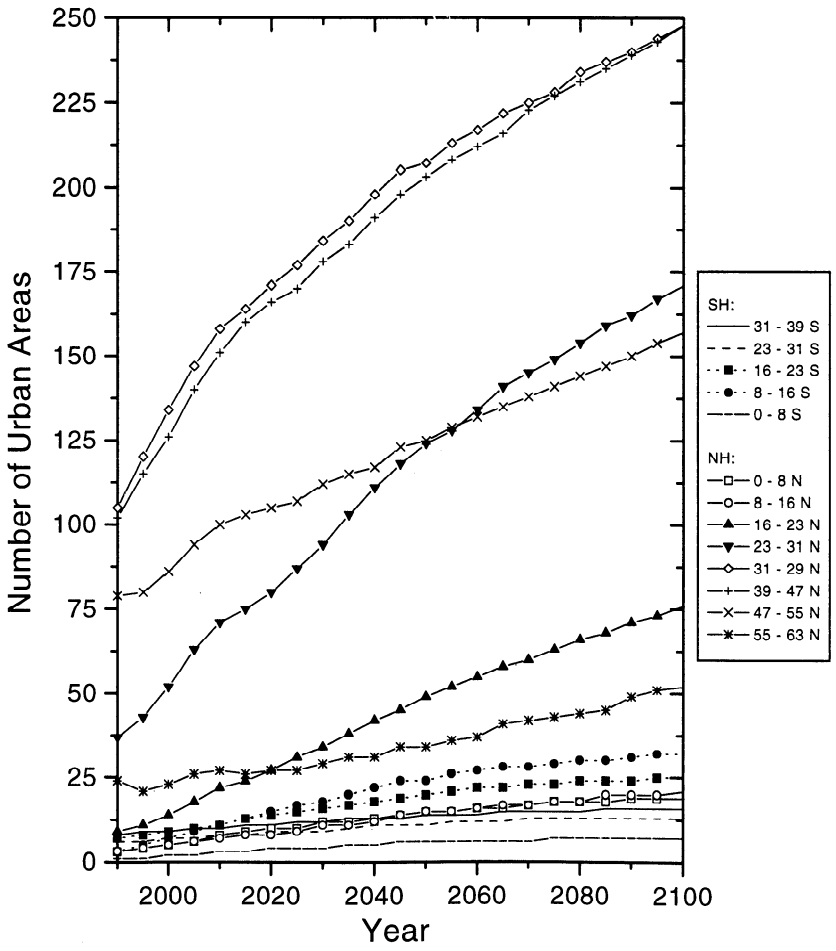

Figure 7. Projected number of polluted urban areas for several latitudinal bands from 1990 through 2100. These projections are used in the META-TIME run.

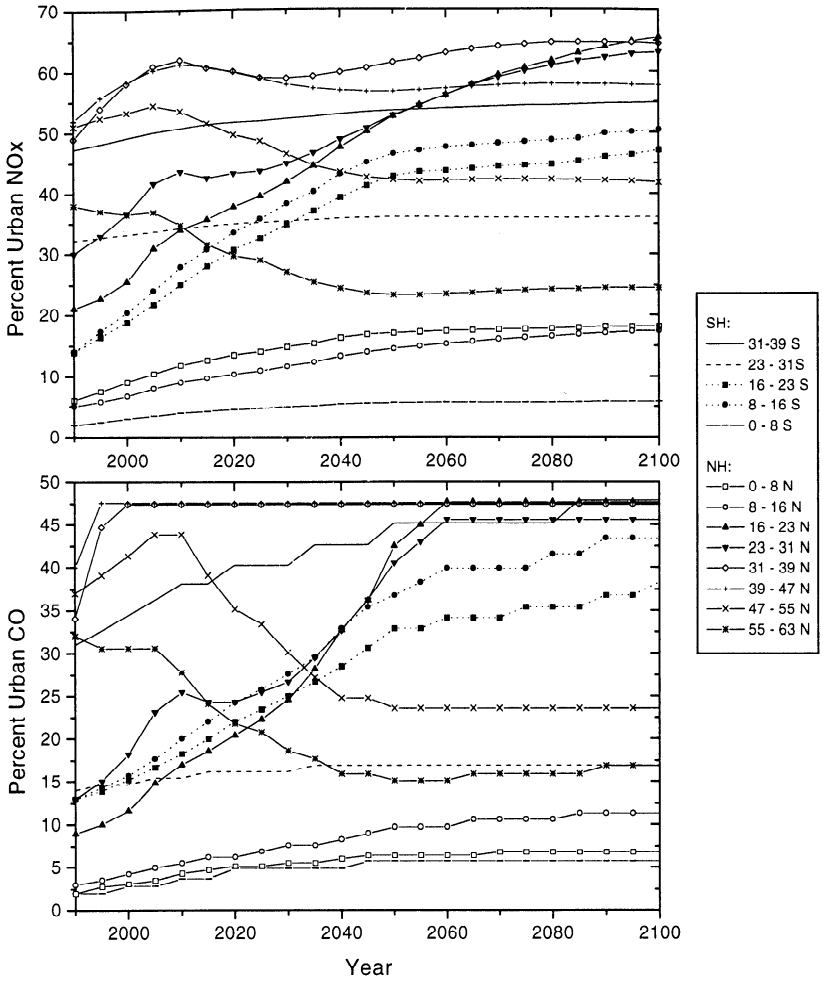

Figure 8. Projected percentage of total NO_x and CO emissions in urban areas for several latitudinal bands from 1990 through 2100. In the META-TIME run these projections are used, whereas in the META run the 1990 values of Table 3 are used throughout 1990 to 2100.

that the shapes of the initial vertical profiles of several species do not change, we can obtain initial and boundary conditions for a compound for a given AQI. These AQIs have a beta distribution ranging from 0 to 1, where 1 denotes a highly polluted atmosphere. The AQI for a species is 1 when the mole fraction reaches 100 ppb for NO, 300 ppb for NO_2, 100 ppb for SO_2, 250 ppb for O_3, 40 ppb for HCHO, 20 ppb for ALD2, 22 ppb for MEK, 95 ppb for ALKA, 28 ppb for ETHE, 18 ppb for ALKE, 20 ppb for TOLU, and 8 ppb for AROM (Table 7 defines these acronyms). [*Finlayson-Pitts and Pitts*, 1986; *Seinfeld and Pandis*, 1998]. For the NMVOC as a whole, the AQI is the sum of the AQIs of HCHO, ALD2, MEK, ALKA, ETHE, ALKE, TOLU, and AROM. To calculate the AQI, the moles of pollutants in urban domains must be converted to mole fractions. The AQI is defined for each species as

$$\mathrm{AQI} = \frac{m \cdot R \cdot T}{p \cdot \xi_{\max}}, \tag{9}$$

where m is the molar concentration of the pollutant in the urban domain, R the gas constant, T the temperature, p the pressure, and ξ_{max} the mole fraction of the species when its AQI is unity.

5. Effect of Local Air Pollution on Global Chemistry and Climate

To investigate the impact of urban air pollution on global chemistry and climate, we carried out three different simulations with the coupled 2D-LO chemistry-climate model. All three runs used the same emissions predictions derived from the EPPA model, which assumes no policy actions to explicitly reduce or cap future anthropogenic emissions. The total emissions of CO and NO_x provided by the EPPA model are shown in Figure 6. (Note that NO_x emissions are expressed in units of Tg N/y, and CO emissions are expressed in units of Tg CO/y.) All three simulations begin in 1977 and end in 2100. The period from 1977 to 1990 is devoted to model spin-up.

The first simulation (the reference run) was done with the 2D-LO global coupled chemistry-climate model, without the reduced-form urban chemistry model. The second and third simulations were carried out using the global model in conjunction with the reduced-form urban model. The two latter runs differed in that, in one case ("META"), the number of urban areas and the percentage of urban emissions were fixed at their 1990 values (see Table 3). Total and urban

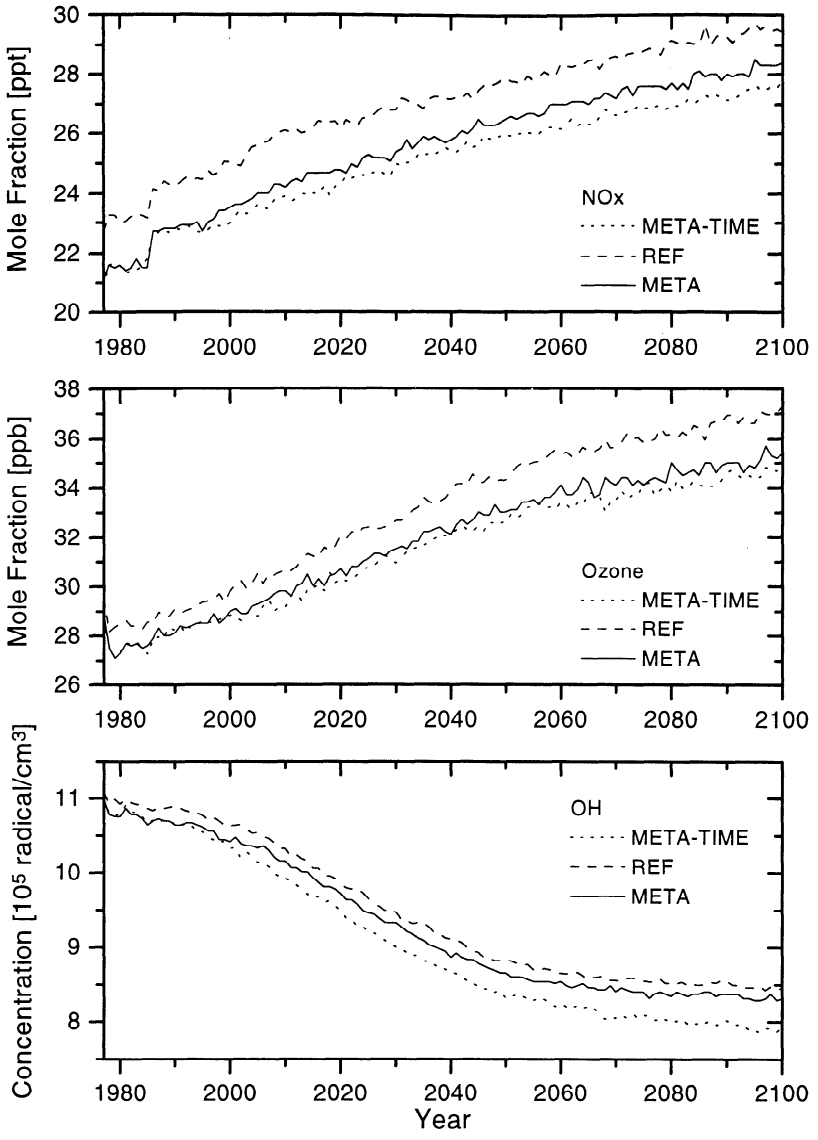

Figure 9. Global average tropospheric (top) NO_x and (middle) O_3 mole fraction and (bottom) OH concentration from 1977 to 2100 for the reference, META and META-TIME runs.

emissions in META were therefore predicted to grow at the same rate. In the other case ("META-TIME") the number of urban areas (Figures 5 and 7) and the percentage of urban emissions were allowed to change through 2100. For META-TIME, the total emissions assumed are the same as in the reference and META runs, but total urban emissions for NO_x, NMVOC, and CO were found to be higher than in the META run. The emissions per city of several pollutants increases substantially over time in the META run. In the META-TIME run, however, the projected number of polluted urban areas increases so that emissions per type of urban area over time remain practically constant. The total predicted number of urban areas in 2100 for the META-TIME run is 2.5 times the number in 1990 (see Figure 5), although for specific latitudinal bands (e.g., 8° – 16°S and 16° – 23°N) the number of cities could be 8 or even 16 times higher in 2100 than in 1990 (Figure 7). Our prediction also shows that in 2100, most urban areas will still be in the Northern Hemisphere midlatitudes. The projected percentage of urban emissions changes substantially over time (Figure 8) primarily because of the increase in urban population (Figure 2). Note that in this study, NMVOC emissions are directly proportional to CO emissions (equation (3)), so urban NMVOC percentages are not calculated separately from percentages for CO.

The effects of including urban processes using the reduced-form model on the global annual average tropospheric NO_x and ozone mole fractions and on the global annual average tropospheric OH concentration are shown in Figure 9 for the META and META-TIME runs. Levels of all three species are found to be reduced compared to the reference run, and the effect on global concentrations is always more significant in the META-TIME run than in the META run. Note that the reason we can see in Figure 9 an immediate difference between the reference run and the two runs using the urban chemistry model is because we plot annual averages, and the lifetimes of all three species in Figure 9 are much shorter than 1 year. The regional reductions in tropospheric ozone when urban chemistry is taken into consideration are much greater

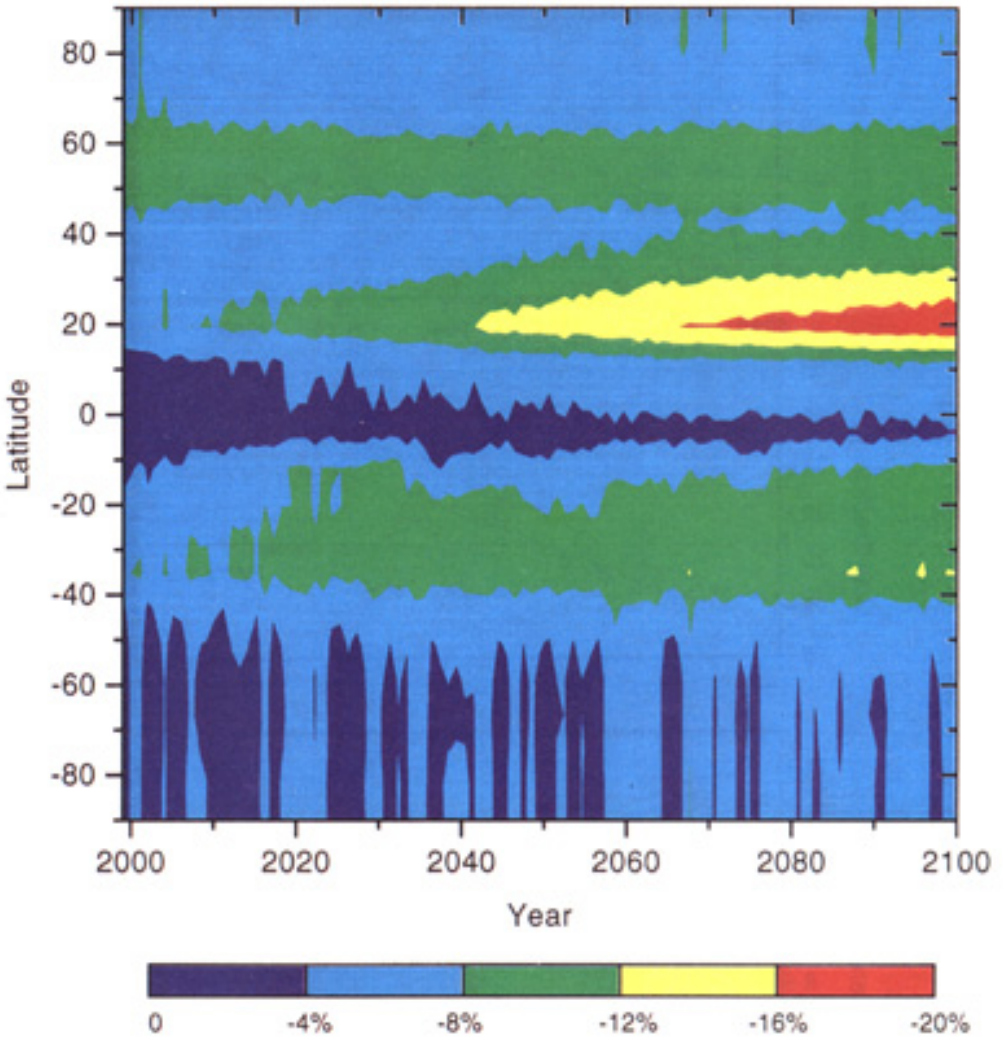

Plate 2. Change in percent of the global average tropospheric O_3 mole fraction for the META-TIME run compared to the reference. Taking urban chemistry processes into account reduces the global tropospheric ozone mole fraction.

(up to minus 20% compared to the reference) than reductions in the global average (up to minus 10%). Plate 2 compares the change in percent for the META-TIME run to the reference run for the period 1999 to 2100. The decrease in ozone is most pronounced at latitudes where large urbanization rates are projected (see also Figure 8).

From Figure 10, we see that the global annual average mole fraction of CH_4 increases faster when urban processes are included, due to the greater decrease in the average tropospheric OH concentration in the two urban cases. The global annual average tropospheric CO mole fraction is also shown in Figure 10. Depending on the scenario for urban area development, we see either a slightly smaller CO mole fraction in the META run or a higher CO mole fraction in the META-TIME run after 2030.

Changes in the global tropospheric mole fractions of ozone and methane influence radiative forcing. Our simulations show an increase in CH_4 and a decrease in O_3 in the troposphere, to different extents, in the two runs that include urban processes. For example, in 2100 the tropospheric averaged mole fraction of CH_4 is about 0.5 ppm higher (META-TIME run) or 0.2 ppm higher (META run) than in the reference run. Figure 10 shows the change in annual mean global surface temperature relative to the annual mean global surface temperature of 1990 for the period 1977 through 2100. If we fix the number of urban areas (META run), we are unable to see a clear change in surface temperature compared to the reference run. Altering the number of cities (META-TIME run) gives slightly higher surface temperatures after 2050. In order to understand the differences between the two simulations, META and META-TIME, we analyzed fluxes and mole fractions in the urban domains for NO_x and NO_y species (in this study, NO_y refers to the sum of PAN, HNO_3, HONO, and N_2O_5), CO, and ozone.

5.1. NO_x and NO_y

We assumed that of the total urban NO_x emissions, 95% is emitted as NO and 5% as NO_2. Figure 11 shows the total emissions of NO, NO_2, PAN, and HNO_3 after chemical processing from urban areas (we will call these "aged"

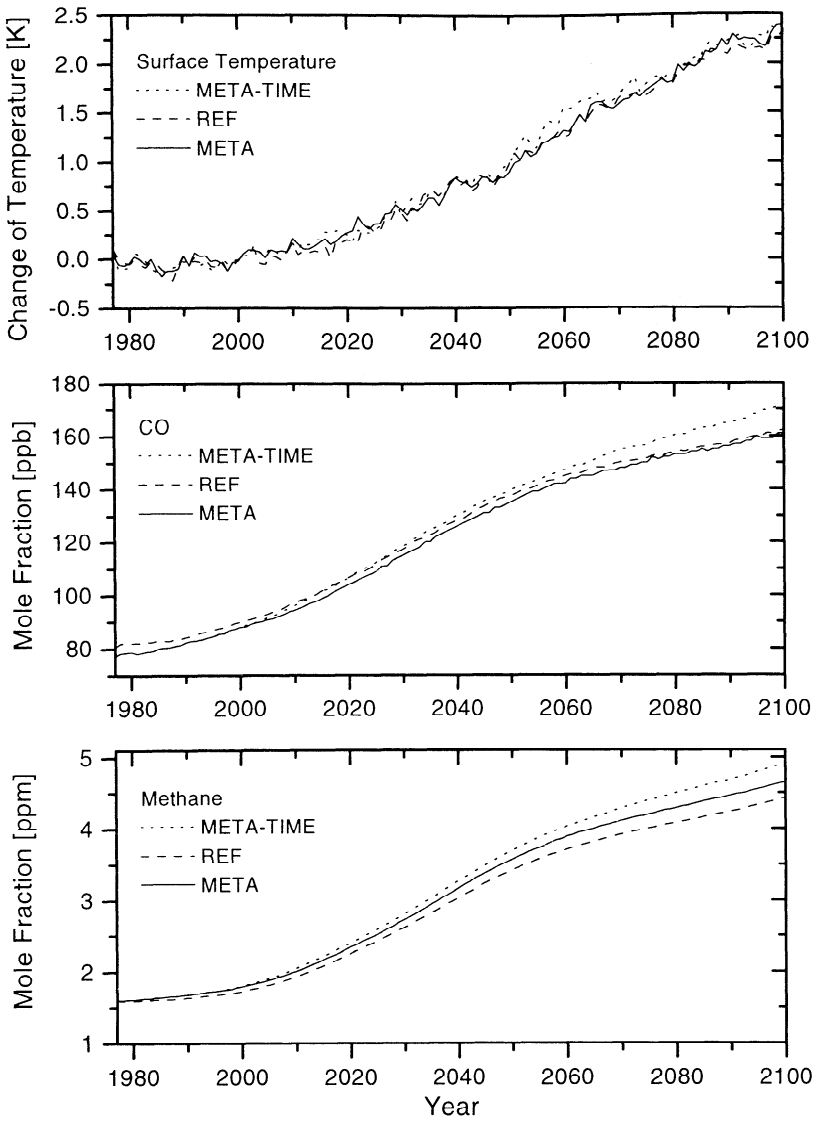

Figure 10. (top) Global mean surface temperature, global average tropospheric mole fractions of (middle) CO and (bottom) methane from 1977 to 2100 for the reference, META, and META-TIME runs. The global mean surface temperature is shown relative to the global mean surface temperature of the reference run in 1990.

emissions) as functions of latitude in 1990, 2050, and 2100 for the META-TIME run. The aged emissions are the aggregated fluxes from the 24-hour simulation (see (7) and related text) averaged over the three city types (low, medium, and highly polluted). All fluxes are expressed in units of Gg N/d. In our analysis PAN is the dominant species of aged emissions in the Northern Hemisphere, and NO_2 is the dominant species in the Southern Hemisphere. In 2100 the flux of all aged nitrogen-containing species is about double that in 1990. In addition, the latitudinal distribution of the fluxes changes over time: more weight is found at lower latitudes in the Northern Hemisphere. The aged emissions shown in the top panel (for 1990) of Figure 11 are also the results for the META run since in that year the same assumptions regarding urban emissions apply to the META and META-TIME runs. For the META-TIME run the aged emissions of NO_y increase proportionally to NO_x emissions, whereas in the META run, NO_y fluxes and their latitudinal distributions do not change to that extent.

The differing behaviors of aged emissions in the META-TIME and META runs are due to the strong nonlinearity of the chemistry. This can be seen more clearly in the temporal behavior of the fluxes from the urban areas and in the mole fractions of NO, NO_2, PAN, HNO_3, HONO, and N_2O_5 in the urban domains (Figure 12). The mole fractions shown in the bottom panels are the 24-hour and urban domain (200 km x 200 km x 2 km) averages for all three types of cities and all latitudinal bands. (Note that actual surface mole fractions are higher than these averages.) Fluxes in the META-TIME run increase with time, mainly due to the increase in the number of cities. Mole fractions, however, fluctuate throughout the simulation and do not show the same significant increase as is apparent for fluxes. The NO mole fraction varies most obviously among all nitrogen-containing species with sudden changes coinciding with the introduction of a new type of city in one or more latitudinal bands. This causes a different allocation of the emissions between low, medium, and highly polluted cities within a latitudinal band leading to different

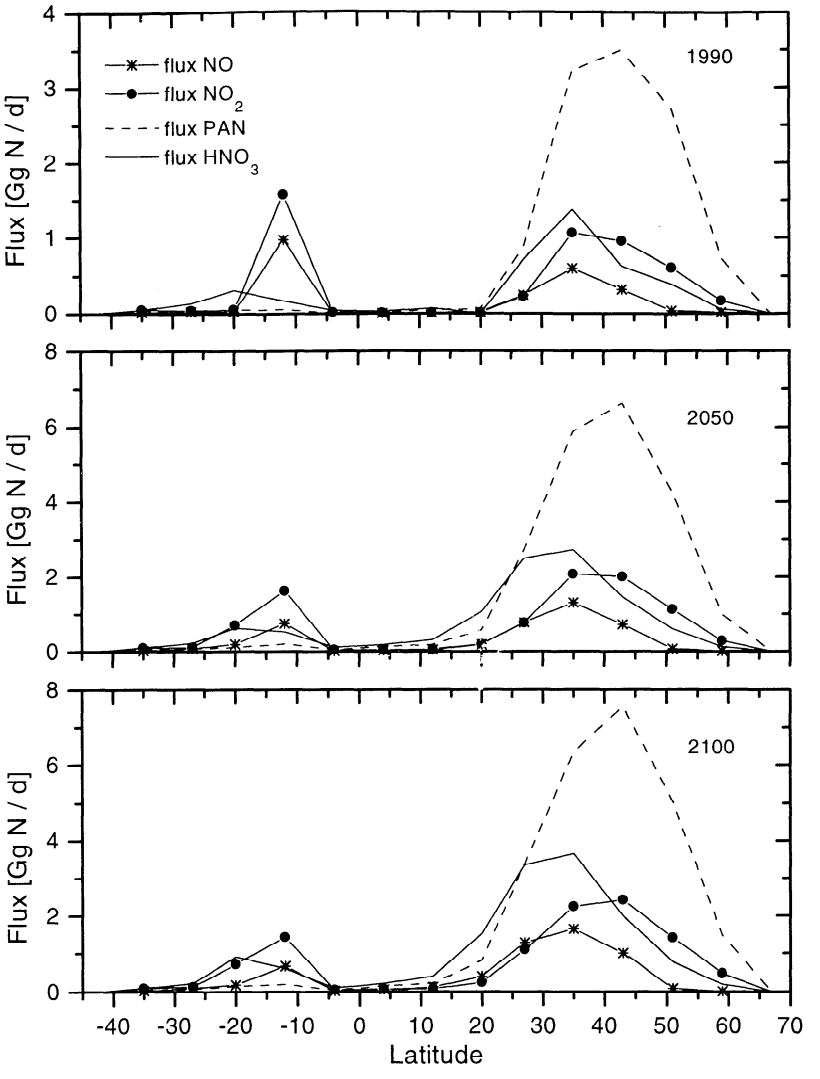

Figure 11. Latitudinal distribution of the annual average fluxes of NO, NO_2, PAN, and HNO_3 exported from urban domains after chemical processing for the META-TIME run for 1990, 2050, and 2100. Note that in 1990 the vertical axis extends only to 4 Gg N/d whereas in 2050 and 2100 it reaches 8 Gg N/d.

average mole fractions for that band. Because we calculate the global average mole fraction as the arithmetic mean of the 13 latitudinal average mole fractions, transitions from an urban scenario with only type 1 cities to a scenario with type 1 and type 2 cities (i.e., from three to four cities) in a single latitudinal band can be seen in the global average (NO_x emissions in medium polluted urban areas are about 2 times higher than in low polluted urban areas). The more cities we project over time the smaller the fluctuations become because eventually in almost all latitudinal bands the three types of urban areas are represented, a situation that is also reflected by an increase in the pollution index plotted in Figure 5. The abrupt changes observed in mole fractions coincide with the changes in the pollution index for the time period after 1990. In the real world, of course, smooth variations would be observed.

The behavior of the mole fractions of NO_x and NO_y in the META run differs from that of the mole fractions in the META-TIME run discussed above. In the META run the emissions per urban area are increased steadily but no new urban areas are added, so the fluctuations of the mole fractions are smaller. The NO_x mole fraction in the META run actually decreases over time although NO_x emissions increase. In 2100 the mole fractions of all NO_y and NO_x species predicted by the META run exceed those predicted by the META-TIME run with the exception of PAN and NO_2.

5.2. Ozone

Plate 3 plots the latitudinal distribution of the annual mean 1-hour peak ozone mole fractions averaged over all three types of urban areas for the META and META-TIME runs for the period from 2000 to 2100. For the META-TIME run we find that at latitudinal bands where initially all three types of urban areas are present (e.g., northern midlatitudes), the peak ozone is quite constant over time due to our assumption that the emission rates for each type of urban area do not change over time. In contrast, at latitudinal bands where we introduce medium and/or highly polluted urban areas during the course of the run, the peak ozone increases abruptly (the pollution index also changes, as Figure 5 shows). The aggregated ozone

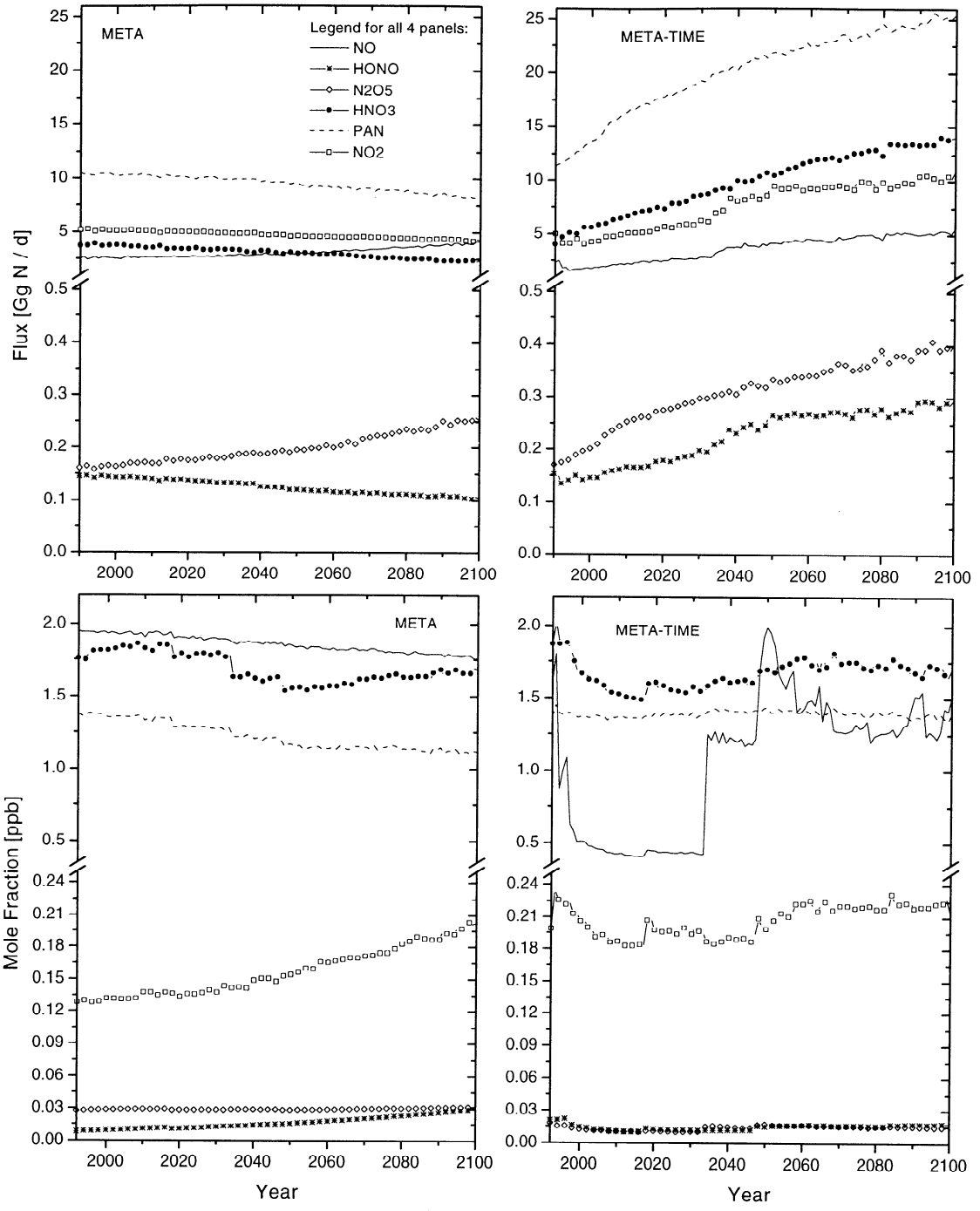

Figure 12. Global annual average fluxes exported from urban domains and mole fractions in urban domains for NO, NO_2, PAN, HNO_3, HONO, and N_2O_5 in the META and META-TIME runs from 1990 to 2100.

luxes grow as urban areas increase in the META-TIME run roughly, by a factor of 3), in contrast to the decrease in ozone luxes found in the META run (Plate 3).

Ozone production is expected to be in the so-called 'NMVOC limited range" [*Duncan and Chameides*, 1998; *Sillman*, 1999] in most urban areas. Therefore an increase in he NO_x mole fraction should not necessarily lead to a higher ozone concentration. A scatterplot of 24-hour and domain average NO_x and NMVOC mole fractions versus 1-hour peak ozone mole fraction is shown in Figure 13 for both the META and META-TIME runs for the data obtained for the period 1990 through 2100. The NO_x, NMVOC, and O_3 mole fractions are the average of the three types of urban areas but not the average of several latitudinal bands. Although in the META run (open symbols), both NO_x and NMVOC emissions in cities grow over time, the NO_x mole fraction decreases (see also Figure 11) in areas where the NMVOC mole fraction is increasing at the same time. The peak ozone is found to be higher with higher NMVOC mole fractions. In the META-TIME run (asterisks and solid squares), the NO_x mole fractions vary significantly (see Figure 11) but the ozone mole fractions change little, due to the quasi-constant NMVOC

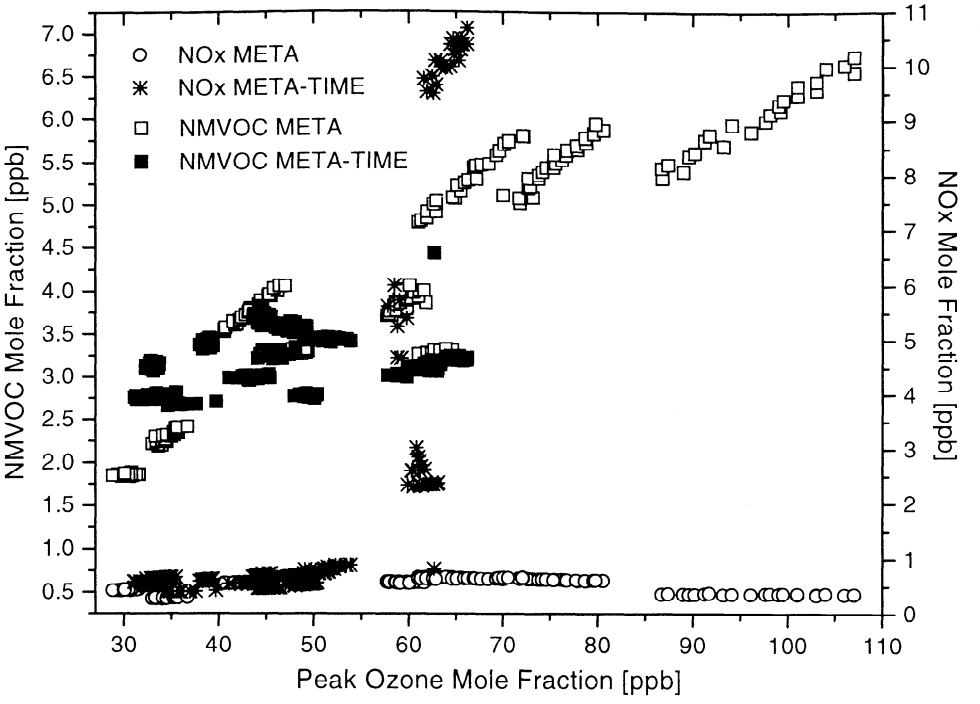

Figure 13. Annual average NMVOC and NO_x mole fractions in urban domains versus peak ozone mole fraction for the META and META-TIME runs. For definition of the NO_x, NMVOC, and peak ozone mole fraction, see text. This analysis suggests that the ozone production in the urban areas is NMVOC-limited.

mole fractions. These results suggest that the urban atmospheric chemistry predicted by our model is indeed within the NMVOC limited regime.

5.3. CO

The CO fluxes from cities increase substantially in the META-TIME run, while they grow only little in the META run. The CO mole fractions increase in both runs, although more so in the META run. Figure 14 plots the fluxes and daily average surface mole fractions over the urban domains for the two simulations. Fluxes and mole fractions are given as the global average of all three types of urban areas.

5.4. Discussion

Allocating emissions as we have done in the META and META-TIME runs provides two extreme scenarios for emissions strengths in urban areas. In the META-TIME run, conversion of NO_x to NO_y proves to be much more efficient than in the META run; therefore less NO_x is available to rural areas on a global scale. Table 9 lists the ratios of NO_y to NO_x for the two runs in 2000, 2050, and 2100, for both fluxes (moles/time) from urban domains and moles within these domains. To facilitate calculation of the ratio NO_y to NO_x, we express all nitrogen-containing species in terms of their nitrogen content. The more NO_x is converted to NO_y, the higher is the value of the ratio derived. In the META-TIME run, the NO_y to NO_x mole ratio declines over time, due to a relative increase in the number of medium-polluted and highly polluted cities with higher NO_x emissions in 2050 and 2100, compared to the initial distribution in 1990.

Global as opposed to urban tropospheric ozone mole fractions are basically determined by the available NO_x. Although urban domains produce more ozone when we implement the urban chemistry model, the global tropospheric ozone mole fraction is lower in the two META cases than in the reference case because of their lower global NO_x mole fractions. In both runs with the urban chemistry model the effective total NO_x emissions (rural emissions plus the flux of NO_x out of urban areas) to the global model are lower than in the reference case. This is primarily due to the efficient conversion of NO_x to HNO_3 and N_2O_5 (NO_2 and HNO_3 fluxes are roughly the same; see Figure 12) in urban areas, where both species serve as sinks for NO_x. At the low average NO_x mole fractions (< 1 ppb) predicted by the global model, changes in NO_x are not expected to alter the ozone production per unit NO_x per day [e.g., *Liu et al.*, 1987] and ozone should follow proportionally the NO_x trend (in our case, about a 7% decrease in NO_x and O_3). Ozone is one main factor determining OH; therefore, together with lower O_3 mole fractions, we also observe lower OH concentrations (note that other factors influencing OH concentration such as CO, CH_4, and water vapor content or radiation change over time, but have a relatively smaller effect than these other factors).

This suggests that global-scale models that do not take into account urban areas' highly nonlinear atmospheric chemistry most likely overestimate tropospheric ozone production due to unreasonably high background NO_x concentrations. Several investigators [e.g., *Duncan and Chameides*, 1998; *Roselle and Schere*, 1995; *Chameides et al.*, 1992; *Sillman et al.*, 1990; *Lin et al.*, 1988] have addressed this issue and reached the same conclusion. Our contribution is a computationally efficient, accurate parameterization of urban chemistry that allows a quantitative estimation of the effects of urban versus rural emissions in a global model. Note also that adding the reduced-form urban model to our global 2-D model enables a substantial amount of the total NO_x emissions to be processed more reasonably. As a result the distribution of the remaining

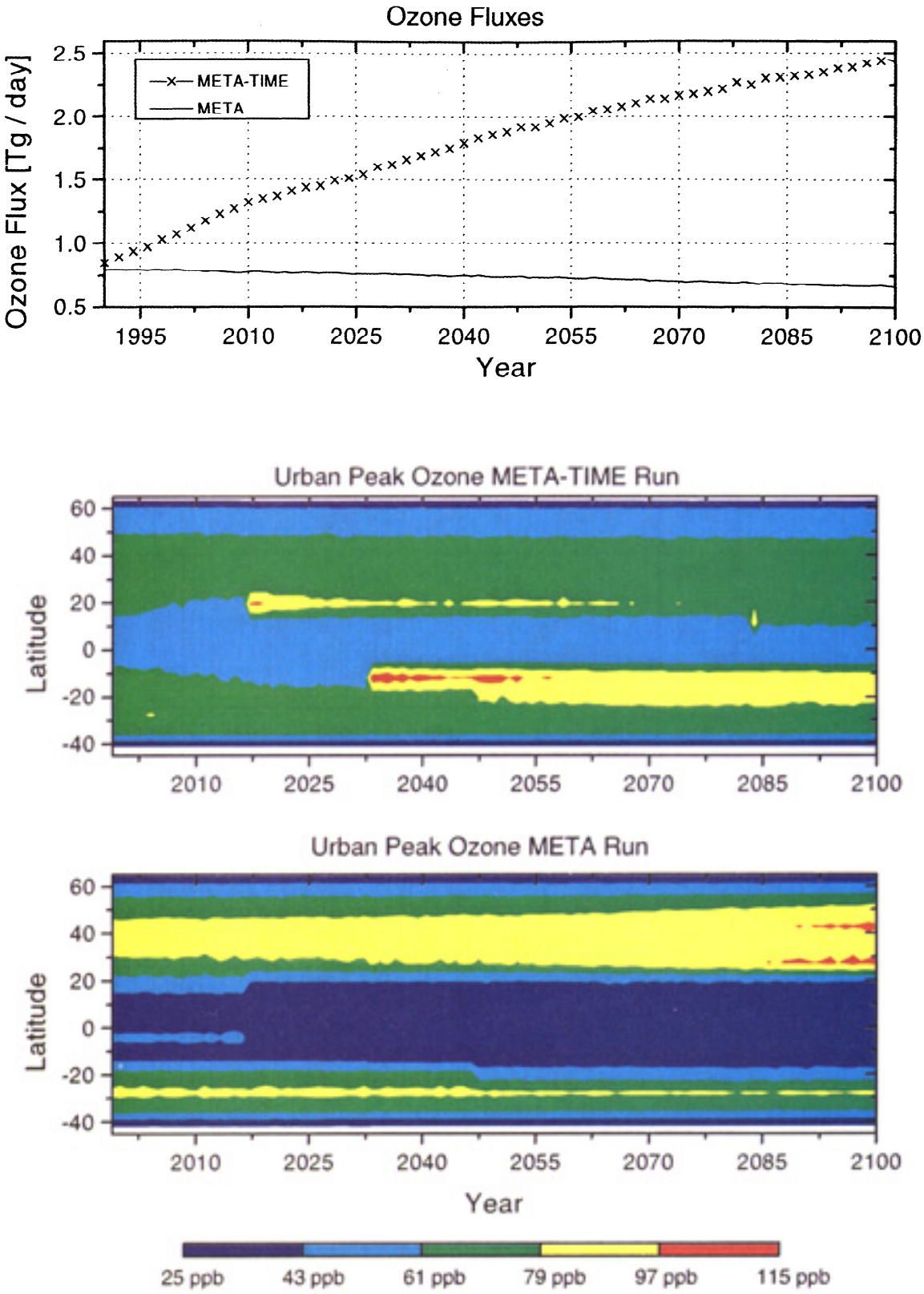

Plate 3. (top) Global annual average ozone fluxes exported from urban domains from 1990 through 2100 and the latitudinal distribution of the annual average peak ozone mole fractions in urban domains for the (middle) META-TIME and (bottom) META runs from 2000 through 2100.

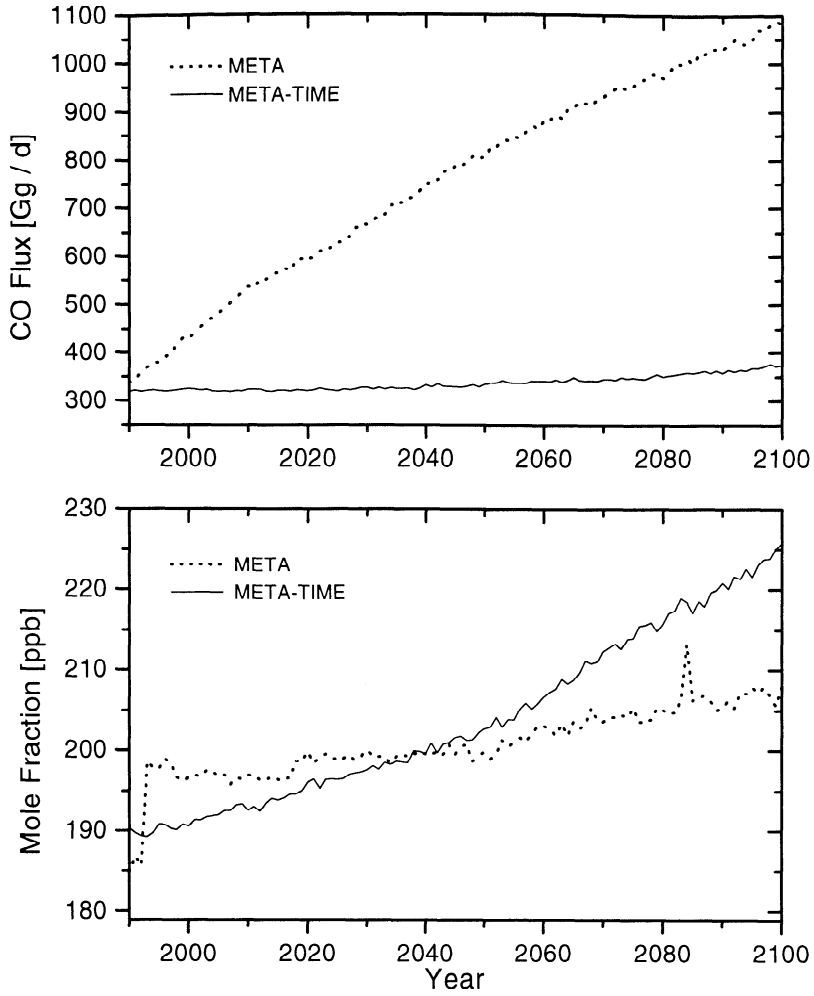

Figure 14. (top) Annual average CO fluxes exported from urban domains and (bottom) surface mole fractions in the urban domains for the META and META-TIME runs from 1990 to 2100. For definitions of the CO flux and mole fraction, see text.

rural NO_x emissions should have a significantly smaller latitudinal gradient. Under this circumstance, the difference between a 2-D global model's results and those of a 3-D model should be reduced, assuming that urban emissions are treated properly in our 3-D urban (CIT) model.

Compared to the reference run, the global tropospheric CO mole fraction does not change substantially as a result of urban chemistry in the META simulation. Despite an additional CO source from NMVOC emissions a slightly lower global average tropospheric CO mole fraction is found in the META run through out the whole simulation. The reduction is attributed to the very efficient CO oxidation in urban areas, which are characterized by relatively high OH concentrations. As a result, less CO is emitted to the global troposphere. The global average CO mole fraction in the META-TIME run is lower than in the reference from 1977 to 2030. After 2030 the global CO mole fraction in the META-TIME run is higher compared to the reference run. The CO fluxes from urban domains grow over time not only because of an increased number of cities, but also because of the relative growth in urban CO and NMVOC emissions. Therefore more CO is released from urban to rural areas in the global model. At the same time, the global OH concentration falls constantly, and the methane mole fraction increases constantly. Both factors (the increasing fluxes and the increasing lifetime of CO) lead eventually to higher global CO mole fractions [e.g., *Wang and Prinn*, 1999].

Table 9. Ratio of NO_y to NO_x Fluxes (Moles/Time) Out of the Urban Domains and the Ratio of NO_y to NO_x Moles Within the Urban Domains Derived for the Cases META and META-TIME for the Years 2000, 2050, and 2100

	META		META-TIME	
Year	Fluxes	Moles	Fluxes	Moles
2000	2.1	1.2	2.7	5.4
2050	1.8	1.2	3.1	2.1
2100	1.7	1.3	2.7	1.9

6. Summary

We have derived a "reduced-form" model or "parameterization" for urban air chemistry based on the California Institute of Technology–Carnegie Institute of Technology (at Carnegie Mellon University) Urban Airshed

Model by employing the probabilistic collocation method. The reduced-form model is computationally efficient and agrees well with the parent urban airshed model over a wide range of input parameters. Incorporating this reduced-form model into the MIT 2D-LO coupled chemistry-climate model enables us to quantify the impact of urban air pollution on global chemistry and climate. By linking an urban airshed model to the 2D-LO global coupled chemistry-climate model we essentially incorporated a high-resolution 3-D model with complex NMVOC chemistry into a computationally efficient global model with O_3-HO_x-NO_x-CO-CH_4 background chemistry that is coupled to a climate model. Up to 50% of NO_x, CO, and NMVOC emissions originate from urban areas, as we have defined these. The remaining ("rural") emissions are now expected to be more evenly distributed, so the average features of the 2-D model should be more realistic approximations than the earlier approach provided. We expect that the use of global-scale model alternatives to ours will lead to qualitatively if not quantitatively similar results.

Three simulations, each including or excluding the reduced-form model, have been carried out for the time period from 1977 to 2100 using identical emissions data. In the two runs involving the reduced-form model, urban emissions of NO_x, NMVOC, CO, and SO_x are allocated in different ways. In one run, the number of cities and the proportion of urban to rural emissions have 1990 values; the constant number of cities and fixed proportion of urban emissions lead to a steady increase in emissions per city. In the other run, we increase both the number of polluted urban areas and the percentage of urban emissions, so that the distribution of city types remains constant over time. These two simulations are compared to the reference, which does not utilize the reduced-form model. We have found that the efficient conversion of NO_x to NO_y, especially to PAN and to HNO_3, in urban areas, leads to lower global tropospheric NO_x concentrations (5% to 10% lower in 2100) than is indicated by the reference run. As a result, the tropospheric mole fraction of ozone and the OH free radical concentration decrease relative to the reference (in 2100, O_3 is 5% to 7% lower, and OH 3% to 7% lower than in the reference run), as well. The tropospheric mole fraction of CH_4 increases relative to the reference (in 2100, 7% to 11% higher) as a result of the lower OH concentration. The tropospheric CO mole fraction is altered up or slightly down due to urban chemistry, the amount depending on the assumptions used for urban emissions. The effect on global mean surface temperature of implementing the reduced-form urban model is not, however, large because the decrease in radiative forcing by ozone is offset approximately by the increase in radiative forcing by CH_4. We are currently preparing to include aged emissions of PAN produced in urban areas into the global coupled chemistry-climate model, which could lead to global NO_x concentrations slightly higher than the current results suggest.

Acknowledgments. We thank several MIT colleagues: Gary Adamkiewicz and Gregory McRae who helped with the CIT Model, Sean Fitzmaurice who provided support with emissions calculations, and Judith Stitt who helped edit the manuscript. We also thank Josep Calbo (Universitat de Girona) for assistance regarding the parameterization of the CIT Model. This research was supported through an Erwin Schrödinger Fellowship awarded by the Austrian Science Fund (J1527-GEO) to M.M., and by the National Science Foundation (grants ATM-9523616 and ATM-9610145), the Department of Energy (grants DE-FGO2-94ER61937 and DE-FGO2-93ER61713), and MIT's Joint Program on the Science and Policy of Global Change, which is supported by a number of industrial and government sponsors.

References

Atkinson, R., Gas-phase tropospheric chemistry of organic compounds: A review, *Atmos. Environ., 24A*, 1-41, 1990.

Atkinson, R., D.L. Baulch, R.A. Cox, R.F. Hampson, J.A. Kerr, and J. Troe, Evaluated kinetic and photochemical data for atmospheric chemistry, *J. Phys. Chem. Ref. Data, 21*, 1125-1568, 1992.

Brasseur, G., J.-F. Muller, and C. Granier, Atmospheric impact of NO_x emissions by subsonic aircraft: A three-dimensional model study, *J. Geophys. Res., 101*, 1423-1428, 1996.

Bouscaren, R., Inventaire des Emissions de Pollutants dans L'Atmosphere dans La Communate Europeenne en 1985, Cent. Interprofessionel Tech. d'Etude de la Pollut. Atmos., Paris, 1990.

Calbo, J., W. Pan, M. Webster, R. Prinn, and G.J. McRae, Parameterization of urban subgrid scale processes in global atmospheric chemistry models, *J. Geophys. Res., 103*, 3437-3451, 1998.

Carnovale, F., P. Alviano, C. Carvalho, G. Deitch, S. Jiang, D. Macaulay, and M. Summers, Air emissions inventory for the Port Phillip control region, *Clean Air, 26*, 134-144, 1992.

Carter, W.P.L., A detailed mechanism for the gas-phase atmospheric reactions of organic compounds, *Atmos. Environ., 24A*, 481-518, 1990.

Chameides, W.L., et al., Ozone precursor relationships in the ambient atmosphere, *J. Geophys. Res., 97*, 6037-6055, 1992.

Crutzen, P.J., and P.H. Zimmermann, The changing photochemistry of the troposphere, *Tellus, 43AB*, 136-151, 1991.

DeMore, W.B., S.P. Sander, D.M. Golden, R.F. Hampson, M.J. Kurylo, C.J. Howard, A.R. Ravishankara, C.E. Kolb, and M.J. Molina, Chemical kinetics and photochemical data for use in stratospheric modeling; Eval. *11, JPL Publ., 94-26*, 1994.

Dignon, J., NO_x and SO_x emissions from fossil fuels: A global distribution, *Atmos. Environ., 26A*, 1157-1163, 1992.

Duncan, B.N., and W.L. Chameides, Effects of urban emission control strategies on the export of ozone and ozone precursors from the urban atmosphere to the troposphere, *J. Geophys. Res., 103*, 28,159-28,179, 1998.

Finlayson-Pitts, B.J., and J.N. Pitts, *Atmospheric Chemistry: Fundamentals and Experimental Techniques*, 1098 pp., John Wiley , New York, 1986.

Fung, I., J. John, J. Lerner, E. Matthews, M. Prather, L.P. Steele, and P.J. Fraser, Three-dimensional model synthesis of the global methane cycle, *J. Geophys. Res., 96*, 13,003-13,065, 1991.

Harley, R.A., A.G. Russell, G.J. McRae, G.R. Cass, and J.H. Seinfeld, Photochemical modeling of the southern Californian air quality study, *Environ. Sci. Technol., 27*, 378-388, 1993.

Hauglustaine, D., and C. Granier, Radiative forcing by tropospheric ozone changes due to increased emissions of CH_4, CO, and NO_x, in Atmospheric Ozone as a Climate Gas, edited by W. Wang and I. Isaksen, *NATO ASI Ser., 32*, 1995.

Jacob, D.J., Chemistry of OH in remote clouds and its role in the production of formic acid and peroxymonosulfate, *J. Geophys. Res., 91*, 9807-9826, 1986.

Japar, S.M., T.J. Wallington, J.F.O. Richert, and J.C. Ball, The atmospheric chemistry of oxygenated fuel additives: tert-butyl alcohol, dimethyl ether, and methyl tert-butyl ether, *Int. J. Chem. Kinet., 22*, 1257-1269, 1990.

Kato, N., and H. Akimoto, Anthropogenic Emissions of SO_2 and NO_x in Asia: Emissions Inventories (plus errata), *Atmos. Environ., 26A*, 2997-3017, 1992.

Levy, H., Photochemistry of the lower troposphere, *Planet. Space Sci., 20*, 919-935, 1972.

Lin, X., M. Trainer, and S.C. Liu, On the nonlinearity of the tropospheric ozone production, *J. Geophys. Res., 93*, 15,879-15,888, 1988.

Lind, J.A., and G.L. Kok, Henry's law determinations for aqueous solutions of hydrogen peroxide, methylhydroperoxide, and peroxyacetic acid, *J. Geophys. Res., 91*, 7889-7895, 1986.

Liu, S.C., M. Trainer, F.C. Fehsenfeld, D.D. Parrish, E.J. Williams, D.W. Fahey, G. Hübler, and P.C. Murphy, Ozone production in the rural troposphere and the implications for regional and global ozone distributions, *J. Geophys. Res., 92*, 4191-4207, 1987.

Lurmann, F.W., W.P.L. Carter, and L.A. Coyner, A surrogate species chemical mechanism for urban-scale air quality simulation models, *Rep. EPA/600/3-87/014a*, U. S. Environ. Prot. Agency, Research Triangle Park, N. C., 1987a.

Lurmann, F.W., W.P.L. Carter, and L.A. Coyner, A surrogate species chemical mechanism for urban-scale air quality simulation models, *Rep. EPA/600/3-87/014b*, U. S. Environ. Prot. Agency, Research Triangle Park, N. C., 1987b.

McRae, G.J., W.R. Goodin, and J.H. Seinfeld, Development of a second generation mathematical model of urban air pollution, I, Model formulation, *Atmos. Environ., 16*, 679-696, 1982.

Olivier, J.G.J., A.F. Bouwmann, C.W.M. van der Mass, J.J.M. Berdowski, C. Veldt, J.P.J. Bloos, A.J.H. Visschedijk, P.Y.J. Zandveld, and J.L. Haverlag, Description of EDGAR Version 2.0: A set of global emission inventories of greenhouse gases and ozone depleting substances for all anthropogenic and most natural sources on a per country basis and on 1° x 1° grid, *Rep. 771060002*, Natl. Inst. of Public Health and the Environ., Bilthoven, Netherlands, 1995.

Pandis, S.N., and J.H. Seinfeld, Sensitivity analysis of a chemical mechanism for aqueous-phase atmospheric chemistry, *J. Geophys. Res., 94*, 1105-1126, 1989.

Perrin, D.D., *Ionization Constants of Inorganic Acids and Bases in Aqueous Solution*, 2nd ed., Pergamon, Tarrytown, N. Y., 1982.

Pickering, K., et al., Convective transport of biomass burning emissions over Brazil during TRACE A, J. Geophys. Res., *101*, 23,993-24,012, 1996.

Prinn, R.G., R.F. Weiss, B.R. Miller, J. Huang, F.N. Alyea, D.M. Cunnold, P.J. Fraser, D.E. Hartley, and P.G. Simmonds, Atmospheric trends and lifetime of CH_3CCl_3 and global OH concentrations, *Science, 269*, 187-192, 1995.

Prinn, R., et al., Integrated global system model for climate policy assessment: Feedbacks and sensitivity studies, *Clim. Change, 41*, 469-546, 1999.

Reilly, J., R. Prinn, J. Harnisch, J. Fitzmaurice, H. Jacoby, D. Kicklighter, J. Melillo, P. Stone, A. Sokolov, and C. Wang, Multi-gas assessment of the Kyoto Protocol, *Nature, 401*, 549-555, 1999.

Roselle, S.J., and K.L Schere, Modeled response of photochemical oxidants to systematic reduction in anthropogenic volatile organic compound and NO_x emissions, *J. Geophys. Res., 100*, 22,929-22,941, 1995.

Saeger, M., et al., The 1985 NAPAP Emissions Inventory (Version 2): Development of the annual data and modelers' tapes, *Rep. EPA-600/7-89-012a*, U.S. Environ. Prot. Agency, Research Triangle Park, N. C., 1989.

Sandnes, H., and H. Styve, Calculated budgets for airborne acidifying components in Europe, 1985, 1986, 1987, 1988, 1989, 1990, and 1991, Meteorol. Synth. Cent. - West, Norw. Meteorol. Inst., Oslo, 1992.

Schwartz, S.E., Gas- and aqueous-phase chemistry of HO_2 in liquid water clouds, *J. Geophys. Res., 89*, 11,589-11,598, 1984.

Seinfeld, J.H., and S.N. Pandis, *Atmospheric Chemistry and Physics: From Air Pollution to Climate Change*, pp. 299-302, John Wiley, New York, 1998.

Sillman, S., J.A. Logan, and S.C. Wofsy, A regional scale model for ozone in the United States with subgrid representation of urban and power plant plumes, *J. Geophys. Res., 95*, 5731-5748, 1990.

Sillman, S., The relation between ozone, NO_x and hydrocarbons in urban and polluted rural environments, *Atmos. Environ., 33*, 1821-1845, 1999.

Smith, R.M., and A.E. Martell, *Critical Stability Constants*, vol. 4; *Inorganic Complexes*, Plenum, New York, 1976.

Sokolov, A.P., and P.H. Stone, A flexible climate model for use in integrated assessments, *Clim. Dyn., 14*, 291-303, 1998.

Spiro, P.A., D.J. Jacob, and J.A. Logan, Global inventory of sulfur emissions with a 1° x 1° resolution, *J. Geophys. Res., 97*, 6023-6036, 1992.

Stockwell, W.R., On the $HO_2 + HO_2$ reaction: Its misapplication in atmospheric chemistry models, *J. Geophys. Res., 100*, 11,695-11,698, 1995.

Tatang, M.A., W.W. Pan, R.G. Prinn, and G.J. McRae, An efficient method for parametric uncertainty analysis of numerical geophysical models, *J. Geophys. Res., 102*, 925-932, 1997.

U.S. Environmental Protection Agency, National air pollutant emission trends, 1990-1996, *EPA-454/R-097-011*, Off. of Air Qual. Plann. and Stand., Research Triangle Park, N. C., 1997.

United Nations, Long-range world population projections: Two centuries of population growth 1950 – 2150, New York, 1992.

United Nations, *World urbanization prospects, The 1996 revision*, New York, 1998.

Wagner, J., R.A. Walters, L.J. Maiocco, and D.R. Neal, Development of the 1980 NAPAP emissions inventory, U.S. Environ. Prot. Agency, Washington, D. C., 1986.

Wang, C., R.G. Prinn, and A.P. Sokolov, A global interactive chemistry and climate model: Formulation and testing, *J. Geophys. Res., 103*, 3399-3417, 1998.

Wang, C., and R.G. Prinn, Impact of emissions, chemistry and climate on atmospheric carbon monoxide: 100-yr predictions from a global chemistry-climate model, *Chemosphere, 1*, 73-81, 1999.

Wang, W., D. Wuebbles, W. Washington, R. Isaacs, and G. Molnar, Trace gases and other potential perturbations to global climate, *Rev. Geophys., 24*(1); 110-140, 1986.

Xiao, X., D.W. Kicklighter, J.M. Melillo, A.D. McGuire, P.H. Stone, and A.P. Sokolov, Linking a global terrestrial biogeochemical model and a 2-dimensional climate model: Implications for the global carbon budget, *Tellus, Ser.B, 49*, 18-37, 1997.

Xiao, X., J.M. Melillo, D.W. Kicklighter, A.D. McGuire, R.G. Prinn, C. Wang, P.H. Stone, and A. Sokolov, Transient climate change and net ecosystem production of the terrestrial biosphere, *Global Biogeochem. Cycles, 12*(2); 345-360, 1998.

Yang, M.S., R.S. Eckaus, A.D. Ellerman, and H.D. Jacoby, The MIT Emissions Prediction and Policy Analysis (EPPA) Model, *Rep. 6*, 49 pp., MIT Joint Program on the Sci. and Policy of Global Change, Mass. Inst. of Technol., Cambridge, 1996.

M. Mayer, R. G. Prinn, C. Wang, and M. Webster, Joint Program on the Science and Policy of Global Change, Massachusetts Institute of Technology, 77 Massachusetts Avenue, Building E40-271, Cambridge, MA 02139-4307. (e-mail: mayer@mit.edu)

(Received December 30, 1999; revised May 1, 2000;
accepted May 11, 2000.)